2016

Microfluidic Device for Motility and Osmolality Analysis of Zebrafish Sperm

Jacob Ethan Beckham
Louisiana State University and Agricultural and Mechanical College

MICROFLUIDIC DEVICE FOR MOTILITYAND OSMOLALITY ANALYSIS OF ZEBRAFISH SPERM

A Thesis

Submitted to the Graduate Faculty of the
Louisiana State University and
Agricultural and Mechanical College
in partial fulfillment of the
requirements for the degree of
Master of Science in Biological and Agricultural Engineering

in

The Department of Biological and Agricultural Engineering

by
Jacob E. Beckham
B.S., Louisiana State University, 2013
August 2016

ACKNOWLEDGEMENTS

First and foremost, I would like to thank my primary advisor, Dr. W. Todd Monroe, for his continued support and guidance. The knowledge I gained during my time as his student is immeasurable in both quantity and worth. I will be forever grateful for the long conversations (most of them way off topic) we had sitting in his office.

Next, I would like to thank my co-advisor Dr. Daniel Hayes. Dr. Hayes has always been ready with advice whenever I've needed it, whether it be on research, business, or life in general. His optimistic pessimism and good humor has made my time in the lab truly enjoyable.

I also offer my thanks to my co-advisor Dr. Terrence Tiersch, for readily providing me with a basis of knowledge on which I can build myself into a noteworthy researcher.

It is with the utmost pleasure that I thank Dr. Marybeth Lima for constantly and unconditionally believing in the version of me that I aspire to one day become. She has shown me that anything is possible if you have the will and determination to see it through.

I would like to thank all of the wonderful and talented people I have had the pleasure to work with, most notably Dr. Tom Scherr, Dr. Leticia Torres-Bernal, Amy Guitreau, Shelby Pursley, Nick Totaro, Mohammad Abu-Laban, Nick Poche, Cong Chen, Lisa Kriegh, Victor Omojala, Gerry Knapp, Lauren Lilly, Faiz Alam, and Cerys McCarthy.

I would like to thank my family for their unending support and encouragement-my mother who imparted on me the stubborn determination that has gotten me through many, many late nights, my father who taught me to stay calm and patient amid chaos, and my sister for whom there are far, far too many things to fit on this page.

Finally, I would like to thank Chelsea for showering me with love, support and encouragement every step of the way.

I acknowledge support from the National Science Foundation ARI-R^2 program grant CMMI-096348 and National Institutes of Health grant 5R24OD010441.

PREFACE

The following thesis describes a microfluidic chip that is able to pneumatically drive fluid flow without the need of a syringe pump, consistently activate zebrafish spermatozoa for the purpose of motility analysis, and measure the osmolality of the activated sample on-chip using electrical impedance measurements. The first chapter provides background information on the techniques used and the motivation for which this device was created. The second chapter describes the methods used to design and fabricate the device, as well as the methods used to carry out the experiments needed to validate the device's functions. The results of these experiments are described and discussed in this chapter as well. Chapter 2 is formatted for submission to the Lab on a Chip journal. The third chapter provides conclusions and recommended future work for continued development and testing of lab-on-a-chip devices for aquatic gamete analysis.

TABLE OF CONTENTS

ABSTRACT

An increasing number of laboratories are evaluating sample quality via motility analysis by means of computer-assisted sperm analysis (CASA) after sperm activation by manual dilution and mixing. Even with the use of CASA, due to user variation, there is a lack of control over the activation process, resulting in inconsistent motility analysis. Low sample volume (~1-2μL), and a short motility duration (burst motility of less than 15s) add to the complexity of these difficulties. The objectives of this study were to develop a microfluidic device with the capabilities to (1) standardize the method of activation for zebrafish sperm so that all cells in a sample are subjected to the conditions needed to activate in a reproducible way, (2) reproducibly enable motility analysis of the activated sample within 5 s after activation without the interference of bulk fluid flow, and (3) facilitate the generation of activation curves by relating osmolality of the sample solution to percent motility at the time when motility analysis was performed. The device described here is a three-inlet microfluidic platform fabricated from polydimethylsiloxane (PDMS) bound to a glass substrate with a microfabricated gold floor electrode for osmolality detection. A passive micromixer is utilized to activate sperm samples, and a novel flow control system was designed to aid with the demands of sample analysis. The device demonstrated consistent zebrafish sperm activation and osmolality detection. The device was also able to consistently reach flow cessation in under 1s, allowing for rapid analysis of the sample. This device represents a pivotal step in streamlining methods for consistent, rapid assessment of sperm quality for zebrafish and other aquatic species. The capability to rapidly activate sperm and consistently measure motility with CASA using the microfluidic device described herein will help improve the reproducibility of studies on germplasm physiology.

CHAPTER 1: BACKGROUND AND MOTIVATION

1.1 Zebrafish as a Biomedical Model

The use of model organisms in biomedical research is an essential tool for gaining critical insight into embryological development and the pathogenesis of human disease. Zebrafish, a robust tropical fish, has become an increasingly popular model for the study of development and pathology over the past two decades. These fish possess many qualities that make them an attractive option as a research model: most notably the ability to apply efficient invertebrate-style genetics to vertebrate-specific questions, and the optical clarity of embryos and larvae which allow easy visualization of developmental processes (Lieschke and Currie 2007). These qualities, coupled with external fertilization, high fecundity, rapid development and high stocking densities, have made zebrafish a primary model in developmental biology (Dooley and Zon 2000). This popularity has led to the generation of thousands of mutant, transgenic, and wild-type zebrafish lines; however maintaining all of these lines as live fish is expensive, inefficient, and logistically complex (Hagedorn, Ricker et al. 2009). The Zebrafish International Resource Center (ZIRC) (University of Oregon, Eugene, OR, http://zebrafish.org) currently houses over twenty six thousand lines. As a solution to these complications, cryopreservation can be utilized to reduce the cost of maintaining myriad live strains, and provide the opportunities for lines to be shared among research laboratories on demand (Tiersch, Yang et al. 2007).

FIGURE 1: Adult Zebrafish (*Danio rerio*). Picture was retrieved from the Zebrafish Model Organism Database (ZFIN), University of Oregon, Eugene, OR 97403-5274; URL: http://zfin.org/; [8 July, 2016].

1.2 Quality Control of Aquatic Sperm

The quality of a given sperm sample can be determined though the examination of several factors including: body condition and nutrition, percent motility, motility duration, the mRNA profile of testicular cells, and membrane and mitochondrial integrity (Yang and Tiersch 2009, Guerra, Valcarce et al. 2013). Current methods for evaluating zebrafish sperm quality remain challenging. Zebrafish sperm have a short motility duration (10-15s burst motility), and each fish yields a small semen volume (1-2 μL) (Yang, Carmichael et al. 2007). As with other aquatic species, zebrafish sperm activate upon exposure to external environmental stimulus. As a freshwater fish, zebrafish sperm activate when exposed to an environment hypotonic to its internal osmolality. To determine the activation osmolality, a range of dilutions is used to evaluate the activation and motility duration as a function of osmolality. The resulting data from these experiments is known as the activation curve (Figure 2). In standard practice, a 300 mOsm/kg solution of Hanks Buffered Salt Solution (HBSS) is used to hold and isotonically dilute zebrafish sperm to prevent sample activation. As the osmolality of the cell solution is varied from 20 to 603 mOsm/kg, there is an inverse correlation between sperm motility and osmolality in sigmoidal fashion, where the highest percent motility is observed at the lowest osmolality (Figure 2). This parameter is useful in determining the optimal osmolality that correlates to the motility duration required by the researcher to evaluate various sperm characteristics. The resulting data can

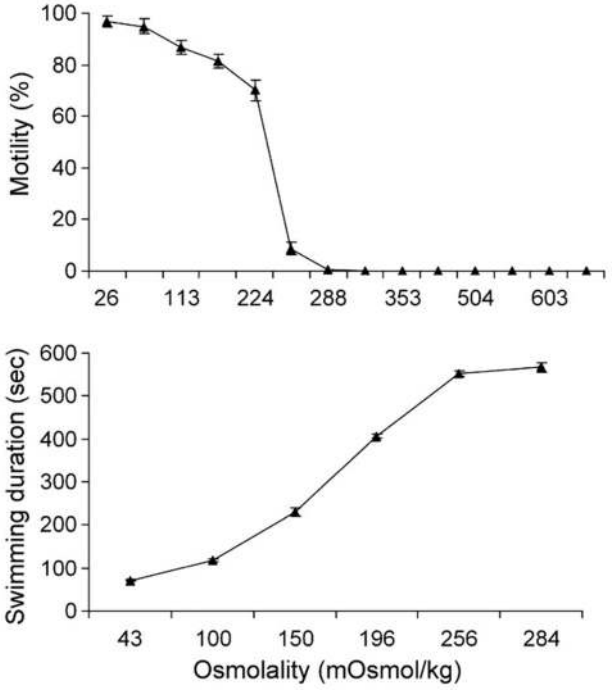

FIGURE 2: (Top) Comparison of percent motility vs. osmolality (Bottom) Comparison of Osmolality and total motility duration of zebrafish sperm suspended in HBSS. Source: Yang et al., 2007

be used in protocol optimization for zebrafish as well as other aquatic species (Yang, Carmichael et al. 2007).

Once activated, zebrafish sperm have only enough energy resources to swim for around 1 min, and sample percent motility begins to drop significantly within 10 s (Wilson-Leedy and Ingermann 2007). This short time window poses a challenge when working with zebrafish sperm. Zebrafish sperm motility analysis requires precise timing, manual activation of sperm, immediate analysis following activation, and careful management of sample quantity due to volume restrictions. Motility analysis is typically performed by activating the sample by manual dilution and hand mixing, and evaluating the motility by visual observation, or through the use of computer assisted sperm analysis (CASA) (Wilson-Leedy and Ingermann 2007, Douglas-Hamilton, Craig et al. 2011). Manual methods reduce the control over activation, and can therefore result in error-prone evaluation of motility. These errors are amplified if subjective visual methods of motility evaluation are used. This lack of standardization decreases the ability for laboratories to recreate experimental results, hindering overall progress.

Visual assessment relies on the technician to sort the sperm into different "grades" by observation alone. Cells are sorted into grade a-d, with "grade a" being rapidly progressive (velocity ≥ 25 μm/s), "grade b" being slowly progressive, "grade c" being flagellating but non-progressive, and "grade d" being immotile. This method was prone to large variations between laboratories due to the technicians inability to assess the velocity of moving sperm (Cooper and Yeung 2006). Semi-CASA systems perform motility analysis by first recording the sperm via a camera mounted onto a microscope. The video is then processed, and simple sperm tracking programs are used to calculate the velocity by the technician 'clicking' on the sperm position in each video frame. However, this method is still subjective since the technician chooses which sperm cells to track, as well as tedious and time consuming (Kime, Van Look et al. 2001). Computer assisted sperm analysis (CASA) is the most objective method for sperm quality analysis,

and automatically assesses sperm motility and sperm velocity (Wilson-Leedy and Ingermann 2007, Douglas-Hamilton, Craig et al. 2011).

Computer Assisted Sperm Analysis algorithms analyze a time window of activity at a predefined frequency (commonly 60Hz) during which the sperm are tracked and analyzed over several different parameters. These parameters include cell size, progressive velocity (VSL), average path velocity (VAP), curvilinear path velocity (VCL), and photo intensity (Figure 3). These parameters must be determined experimentally for a given species. The algorithm can then be optimized to analyze samples within the peak thresholds, i.e. maximum motility for the longest duration. The established parameters allow CASA to distinguish between motile and non-motile sperm, as well as non-sperm objects in the field of view. The CASA system monitors the microscope viewing area for sperm motility and tracks individual cell displacement over time (Figure 3). A motile sperm cell can be assumed capable of its ultimate goal of fertilizing the oocyte. Motility can be classified in several different ways. If a sperm cell is moving its tail, it can technically be considered motile. However, progressive motility is more telling of a sperm cell's potential for fertilization. Progressive motility refers to the track and displacement of the sperm cell. A progressive cell typically moves in a straight overall path with a greater displacement than a non-progressive cell.

Path data is automatically analyzed using the CASA system's specific algorithm and is exported to data files in the project directory. The total movement of all qualifying cells based on set parameters is considered total motility, typically reported as percent motility. Each of these parameters is species-

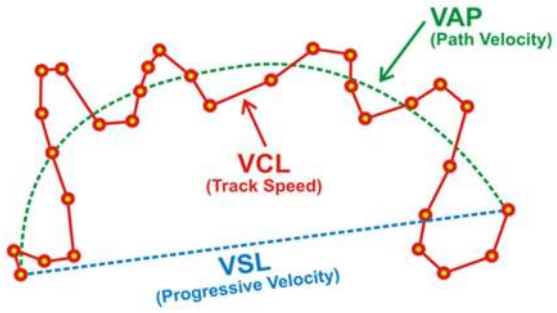

FIGURE 3. Diagrammatic representation of the track of a sperm as analyzed by a CASA algorithm. (Source: Douglas-Hamilton, Craig et al. 2011)

specific and must be determined by experimentally developing a profile for the species in the CASA software (Douglas-Hamilton, Craig et al. 2011). For zebrafish sperm, the CASA parameters have been studied but standardization across the community is lacking. For example, software has been developed for the analysis of fish sperm by creating a CASA plugin for the free National Institutes of Health software ImageJ (Wilson-Leedy and Ingermann 2007). This approach provides a cost-effective method to standardize software across different groups, but results may still vary due to different hardware. This does however indicate progress toward standardization as well as provide methods for further groups to integrate CASA into existing protocols.

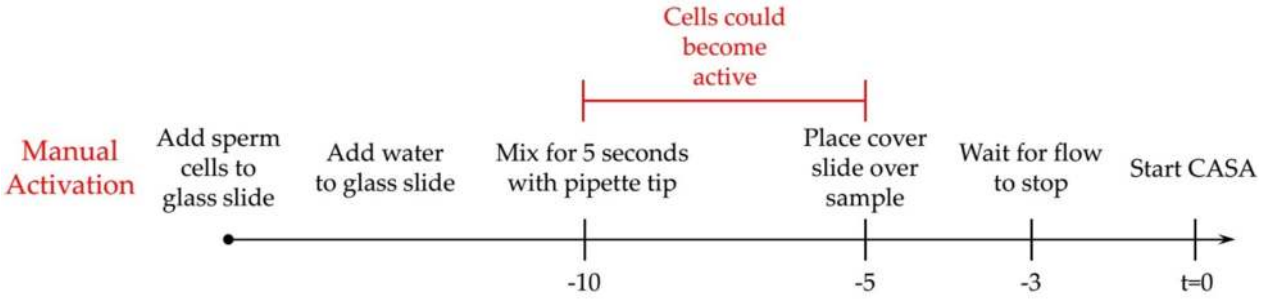

FIGURE 4: A timeline of the cell activation events during manual sperm activation procedure.

While CASA outperforms manual techniques for motility analysis, sources of error are still present in post-thaw motility studies on sperm. In order to gather relevant data on sperm motility, proper and consistent activation of sperm cells is needed. Currently, sperm samples are activated manually by a technician (Wilson-Leedy and Ingermann 2007). This process is done by pipetting sample media onto a glass slide, followed by the addition of water for dilution and sperm activation. The two fluids are then gently mixed using the pipet tip, and the sample motility is analyzed (Figure 4). Because sperm can begin activating as early as the onset of the dilution/mixing step, there is a potential ~10 s latency period before motility analysis can be performed. While a highly trained technician can reduce this latency period considerably, 10 s is a generous estimate that takes into account technicians with a lack of experience using man-

ual activation methods, i.e. newcomers to the field. This time lag results in motility analysis potentially being performed after the initial burst motility has begun to decrease, causing potential errors in motility analysis and determining male reproductive quality. This procedure has been shown to be poorly reproducible by previous studies and produces high variability in results (Figure 5)(Scherr, Knapp et al. 2015). The initial motility of the sample was shown to be ~40%, with a small decrease in motility over time. The standard deviations at each time point were over 50%, indicating that poorly reproducible hand mixing resulted in latent diffusion. It is likely that this diffusion caused sperm cells to activate well after the initial mixing step (Figure 4). Lending to these issues are low sample volumes, and the brief burst motility duration of zebrafish sperm (10-15s), which creates a need for rapid sample analysis. To accommodate the physical demands of zebrafish motility analysis and standardize processes, the current systems could be miniaturized, streamlined, and tailored to handle small sample volumes. Due to its ability to handle small sample sizes and rapidly analyze samples, the field of microfluidics is apt to providing solutions to these hurdles.

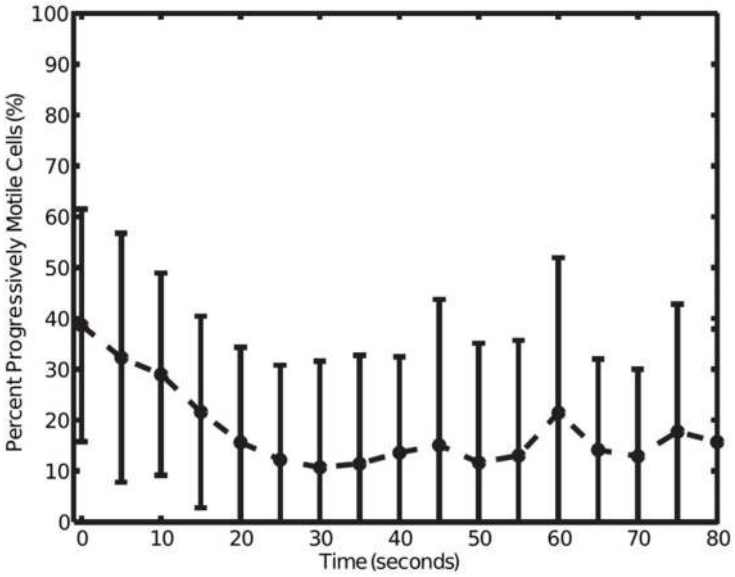

FIGURE 5: Percent motility over time of zebrafish sperm activated using manual activation methods (Scherr, Knapp et al. 2015). (Concentration: $1x10^8$ cells/mL, Dilution ratio: 2:1, n=6)

1.3 Microfluidics and Microfluidic Devices

Microfluidics can be defined as the study of flows that are simple or complex, mono- or multiphasic, which are circulating in artificial microsystems (Tabeling 2005). Microfluidics is a multidisciplinary area of interest that aims to understand and apply the flow and interaction of

fluids that have been geometrically constrained to dimensions on the submillimeter scale. At this scale, power consumption is low, sample volumes are in the nano-liter, or pico-liter range, and the flow of fluid is strictly laminar (Whitesides 2006). The characteristic laminar flow in microchannels is indicated by a Reynolds number that is typically less than unity. The Reynolds number is defined as the ratio of inertial forces to viscous forces, and can be described by $Re = VL/v$, where V is the fluid velocity, L is the characteristic length (or diameter) of the channel, and v is the kinematic viscosity of the fluid.

Because of its small form factor, it is possible to integrate several processes into a microfluidic chip. This allows integration of several steps into one, saving time and reducing sample and reagent quantities. These devices have been labeled as lab-on-a-chip (LOC) or micro total analysis system (μTAS) (Whitesides 2006). There has been extensive investigation and application of LOC technology to various biochemical and cell analysis techniques (Kovarik, Gach et al. 2012). For instance, the utility of microfluidics has been demonstrated in Murine in vitro fertilization (IVF) technology, where there was an increase in fertilization rate of 10-27% in microchannels versus center-well dishes for concentrations of sperm in the range of $2x10^4$-$8x10^4$ cells/mL (Suh, Zhu et al. 2006). Furthermore, microfluidic devices provide a geometrically constrained microenvironment that is similar to the in vivo microenvironment, creating an ideal setting to study the dynamics of sperm and fluid flow interactions (Beebe, Mensing et al. 2002). Studies following this trend have found that the geometry of the microchannel and the flow rate through the device are determining factors for sperm cell behavior during fertilization. It was demonstrated that bovine sperm tend to swim near walls and contours, and will only attempt to fertilize an oocyte when they have overcome the local flow rate (Lopez-Garcia, Monson et al. 2008). A microfluidic device has also been used to sort and orient bovine, murine, and human sperm using hydrostatic pressure (Seo, Agca et al. 2007). Microfluidic devices have also been used to separate human sperm cells from epithelial cells with the prospect of streamlining fo-

rensic analysis in sexual assault cases (Horsman, Barker et al. 2004, Norris, Evander et al. 2009). To date, only two microfluidic devices have been developed specifically for the activation of zebrafish sperm cells for motility assessment, so this field is relatively open for exploration and new contributions (Park, Egnatchik et al. 2012, Scherr, Knapp et al. 2015).

1.4 Mixing at the Microfluidic Scale

The characteristic laminar flow in microfluidic channels creates a daunting challenge in terms of activating sperm samples. While the Reynolds number is typically used to describe flow on the microscale, it may be the least revealing about the problem at hand. A more telling characterization is given by the Peclet number, which describes the ratio of convective transport to diffusive transport. The Peclet number is defined as:

$$Pe = \frac{Uw}{D} \qquad (1)$$

where U is the velocity, w is the width of the channel, and D is the diffusivity. The evaluation of this model for microfluidic channels typically result in Pe>1000, indicating that diffusive transport dominates convection in the channel (Equation 1) (Scherr 2014). This flow characteristic has led researchers investigating LOC technology to develop a variety of integrated micromixers that fall into two categories: active and passive mixers.

Active micromixers involve the use of an external field or force to increase perturbation in fluids present in a microchannel (Hessel, Lowe et al. 2005). These mixers can be effective in a short period but typically are more difficult to fabricate and more costly due to supporting external equipment. Passive micromixers contrast active mixers in that they require simple fabrication techniques, are usually pressure driven, are easy to integrate into existing microfluidic systems, and have no additional power source requirements. These mixers typically utilize specialized channel geometries to increase mixing efficiency by increasing the interface surface

area as to promote further diffusion (Hardt, Drese et al. 2005). Based on the comparison above, this project focuses on the integration of passive micromixers into a microfluidic device.

1.5 Passive Mixers

Several passive micromixers have been designed to produce rapid mixing over a range of Reynolds numbers. These passive mixers have employed several channel geometries such as hydrodynamic focusing, split-and-recombine, sudden expansion and constriction, and chaotic advection (Hardt, Drese et al. 2005). A wide variety of passive micromixers have been developed by exploiting different mechanisms by which to force mixing at the microscale (Hessel, Löwe et al. 2005, Nguyen and Wu 2005). To date, two passive micromixers have been investigated for the activation of zebrafish sperm and are discussed herein: the staggered herringbone mixer (SHM), and the sequential logarithmic mixing apparatus (SeLMA).

The staggered herringbone mixer has become one of the most recognizable passive mixers in modern microfluidics (Figure 6) (Stroock, Dertinger et al. 2002). The mixer utilizes

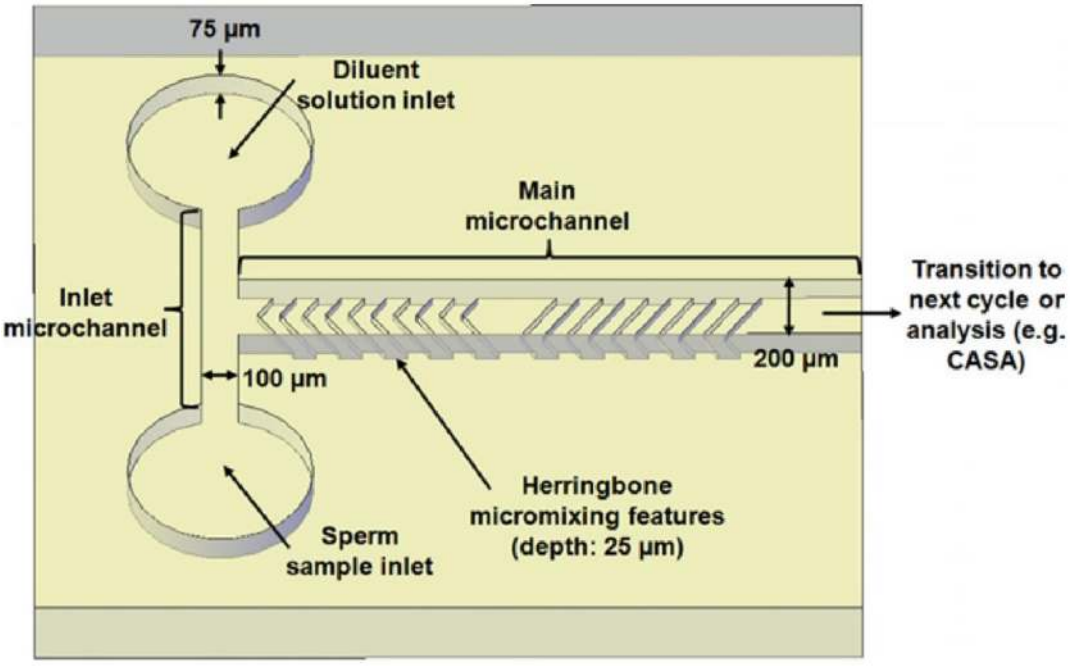

FIGURE 6: A two-inlet herringbone micromixer used for zebrafish sperm cell activation. (Park, Egnatchik et al. 2012)

grooves in a herringbone pattern oriented on the floor or ceiling of the microfluidic channel to create circular secondary flow in the channel as the fluid moves downstream (Stroock, Dertinger et al. 2002). The primary mixing principle exploited by the SHM is chaotic advection; or the stretching and folding of layers of fluids, creating multiple layers and increasing interfacial area and thus efficient mixing. The ability of the SHM to perform well at a wide range of Reynolds numbers (1 to 100) (Nguyen and Wu 2005), has contributed to its prevalent use and status as a performance benchmark for other mixers. The viability of using a two inlet herringbone mixer (Figure 6) for effective zebrafish sperm activation was investigated, and it was found that the sperm activation of the micromixer (56 ± 4% motility) was statistically higher than that of manual hand mixing (45 ± 7%) (Park, Egnatchik et al. 2012).

The Sequential Logarithmic Mixing Apparatus, or SeLMA, is a mixer that has a logarithmic based curvature (Scherr, Quitadamo et al. 2012) (Figure 7). The mixer is designed to integrate multiple mixing principles into one micromixer, such as induced chaotic advection and Dean flows, sudden constriction and expansion, and hydrodynamic focusing of the reagents. SeLMA has three inlets; two sheath streams that are perpendicular to and hydrodynamically focus a central sample stream. The design decision for a log-based curvature is primarily based on a constantly changing cross sectional area of the mixer to the constriction point as well as a changing radius of curvature throughout the log curve. Having two different curvatures for each wall of the mixer allows this constant change to take place. The value in this constantly changing environment is an increasing Re as well as a changing radius of curvature that aids Dean flow (Figure 8). This induces counter-rotating vortices to increase the interface of the reagents to expedite diffusion of the different fluids (Scherr, Quitadamo et al. 2012). Furthermore, the lack of grooves and sharp corners greatly reduces the risk of entrapping sperm within the mixer. It has been shown experimentally that SeLMA has a 10-15% higher mixing efficiency than other passive planar micromixer designs (Scherr, Quitadamo et al. 2012). Activa-

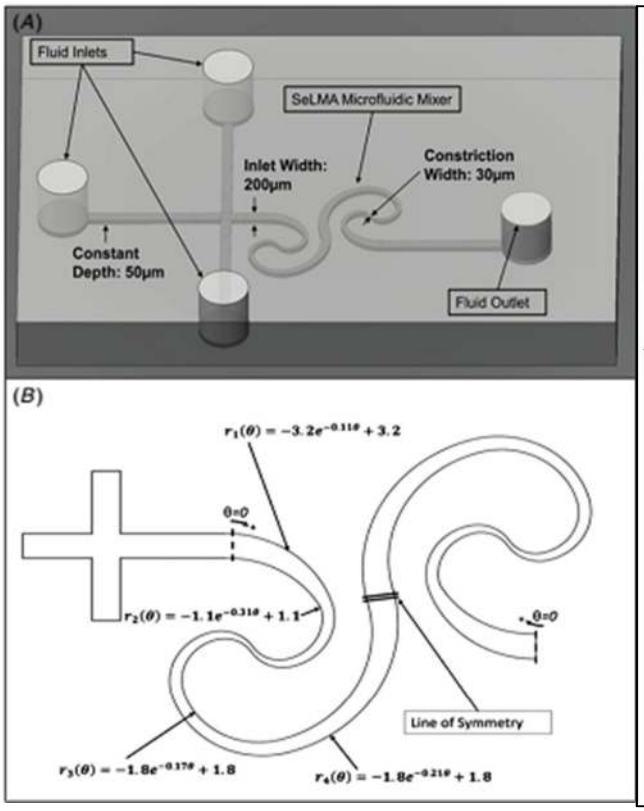

FIGURE 7: Diagram of the SeLMA device schematic showing planar geometry with logarithmic curves to increase mixing by inducing Dean secondary flow vortices. (Scherr et al 2012)

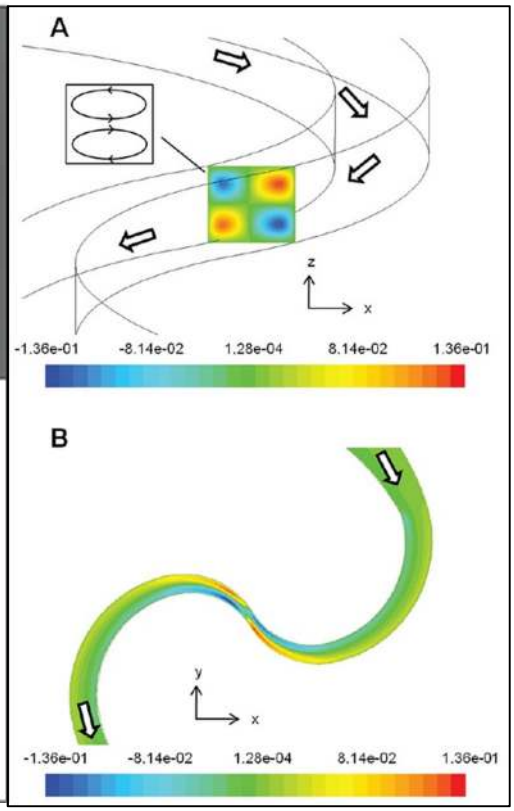

FIGURE 8: Simulation images of z-velocity at the first constriction of the mixer. A) Dean vortices induced at constriction. B) The plane is taken at a constant height of 40 μm from the bottom of the channel. (Scherr, Quitadamo et al. 2012)

tion of zebrafish sperm with this micromixer was demonstrated with a progressive motility of 62% (Scherr, Knapp et al. 2015).

While these microfluidic devices show promise in terms of mixing capability, each has a limited capacity to control fluid flow (Park, Egnatchik et al. 2012, Scherr, Knapp et al. 2015). These studies used a syringe pump to drive flow through the inlets to an open outlet. As a result, backpressure built at the inlets and causes a period of residual bulk fluid flow after the syringe pump was stopped. This residual flow had the potential to skew data by causing immotile sperm caught in the flow stream to appear motile. For a device to work optimally in

conjunction with CASA or other motility analysis methods to analyze zebrafish sperm samples, it is imperative that effective control over fluid flow be achieved.

1.6 Instrument-Free Pumping Mechanisms in Microfluidics

One of the fundamental research themes in microfluidics and LOC technology is the replacement of bulky external equipment with integrated chip-scale technology. Advancement in this area is necessary to further the progress of microfluidics toward a practical and marketable technology. As a result, equipment-free pumping has become an active area of research that has made possible recent developments in on-chip flow control. As explained above, the use of a syringe pump to drive flow through a microfluidic device can result in an undesirable latent period of residual bulk fluid flow. One alternative is to eliminate the syringe pump from the design and implement an integrated pumping mechanism such as those described below to regulate flow.

The recent progress in instrument-free flow control has wide applications in the laboratory setting, as well as in healthcare for point-of-care diagnostics. For example, the "Squeeze Chip" uses a system of check valves actuated by finger squeezing to precisely control flow (Li, Chen et al. 2012). This device was able to provide a quantitative colorimetric analysis of glucose and uric acid concentrations. A similar finger-powered pumping system was used to generate oil-in-water and water-in-oil droplets, as well as to encapsulate endothelial cells in droplets, without the use of external or electrical controllers (Iwai, Shih et al. 2014). 3-dimentional (3-D) printing was utilized to create a series of "pumping lids", which can generate precise positive or negative pressures to drive flow (Begolo, Zhukov et al. 2014). A simple finger-press actuated chip was developed that can isolate CD4+ cells from whole blood via magnetophoresis, providing an inexpensive and instrument-free method for monitoring HIV in resource-poor regions (Glynn, Kinahan et al. 2014).

By analyzing the constraints required to analyze zebrafish sperm motility on-chip, and the way the device is to be implemented, a novel pumping mechanism has been designed to potentially take the place of the syringe pump. This was done by integrating resealable PCR tubes into the inlets of the device, creating a reservoir into which samples can be directly pipetted. These tubes are connected via tubing to a transfer pipette with a relief port in the bulb of the pipette. When the tubes are sealed, and the bulb of the pipette is squeezed, positive pressure is generated and fluid is pushed from the reservoirs towards the outlet of the device. This design will be further described and characterized in Section 2.3.

1.7 Particle Tracking Velocimetry

While the previously described equipment-free pumping mechanism has advantages, it lacks in the ability to precisely control flow rates when compared to traditional methods. Because mixing in a passive micromixer (and therefore sample activation) is dependent on fluid velocity, having the ability to measure and control the flow rate is essential. As will be discussed in Section 2.3, the flow rate will be controlled by varying the amount of pressure applied at the inlets. To measure the flow rate generated by this pressure, particle tracking velocimetry (PTV) was used.

Particle tracking velocimetry is a Lagrangian technique that measures the velocity of a fluid by tracking the motion of particles suspended in the fluid. To determine the fluid velocity, micro-particles flowing through the channel are recorded and the trajectory of each particle is tracked. The displacement of the particles is measured with respect to a known period of time. This versatile technique is widely used in microfluidics to measure flow properties. Particle tracking has been used to measure flow generated by bioinspired cilia (Chen, Cheng et al. 2015), and to determine the relationship between slip length and the concentration of colloidal hard spheres flowing through microchannels (Ghosh, van den Ende et al. 2016). The flow rate in the sperm analysis device was measured using the 2D/3D Particle Tracking plugin for ImageJ. This

plugin uses a feature point tracking algorithm to detect particle trajectories in an image sequence (Sbalzarini and Koumoutsakos 2005). This program detects particles based on their relative intensity value, and can handle particle appearance and disappearance, making it ideal for tracking multiple particles as they flow through a microfluidic device.

1.8 Impedance Spectroscopy

As addressed in Chapter 2, to aid in the development of a standardized motility analysis protocol for zebrafish sperm, it is necessary to investigate the effects of sample osmolality on motility initiation and duration though the generation of an activation curve (Figure 1). Osmolality is typically evaluated in a freezing point depression osmometer. The freezing point method operates on the principle that as the concentration of a solute dissolved in a solvent increased the freezing point of the solution decreases. By measuring the freezing point of the solution, the osmolality, or concentration, can be determined. However, this method is time consuming, and (if cells are present) destructive to the sample. Because of these drawbacks, other osmometry techniques should be considered, particularly those amenable to miniaturization and incorporation on-chip. It is possible to evaluate the osmolality of a solution indirectly by measuring the impedance generated by passing a current through the solution via a simple electrode. Impedance can be defined as the total opposition a circuit offers to the flow of an alternating current (AC) at a given frequency.

Impedance spectroscopy (IS) is a general term that subsumes the small-signal measurement of the linear electrical response of a material of interest (including electrode effects) and the subsequent analysis of the response to yield useful information about the physicochemical properties of the system. (Macdonald 1992)

In practice, IS is performed by measuring the impedance of a sample between two electrodes, which can be defined as: $Z = \frac{V}{I}$, where V is the AC voltage and I is the complex current. Impedance has two components, a real (or resistive) part and an imaginary (reactive) part. This can be represented in either rectangular coordinate form by the resistive (R) and reactive (X)

($Z = R + jX$), or in polar coordinate form as a magnitude and phase angle (θ) ($|Z| = \left|\frac{V}{I}\right|$ and $\measuredangle Z = \theta$). In polar form, the magnitude refers to the resistive portion of the impedance measurement, while the phase angle refers to the reactive part. The phase angle can be used to determine if a circuit is exhibiting inductive or capacitive behavior. If the phase angle is negative, it indicates capacitive behavior, while a positive phase angle indicates inductance.

Impedance Spectroscopy can be divided into two main categories: The first is Electrochemical Impedance Spectroscopy (EIS), which deals with the analysis of materials in which ionic conduction strongly predominates (Macdonald 1992). The second category is concerned with everything else, which can be crudely lumped into the analysis and characterization of the dielectric properties of a sample as a function of frequency(Audiffred 2012). This technique has wide applications in biosensors, such as quantifying hematocrit, determining the osmolality of a solution, determining sperm concentration in semen, and label-free detection of live and dead cells (Futai, Gu et al. 2004, L.I. Segerink 2009, Audiffred 2012). Because the HBSS solution used to dilute zebrafish sperm cells contains salts which impart conductivity proportional to their concentration, EIS will be an ideal technique to determine sample osmolality. This technique will be applied to the device proposed through the integration of a two gold micro-electrodes into the floor of the microchannel, enabling repeated measures of osmolality as fluid and cells progress through the microfluidic device.

1.9 Surface Modification of PDMS Microfluidic Channels

Because zebrafish sperm are prone to adhering to surfaces after they become immotile, it may be necessary to modify the surface chemistry of the microfluidic channel in the device. Altering the surface of a PDMS-based microfluidic channel is a widely used technique that can facilitate reactions, protect the device from damage, as well as trap cells and molecules of interest. However, a large portion of the research into PDMS surface modification is directed towards reducing the hydrophobicity of the material. This hydrophobicity is exacerbated by a

fast hydrophobic recovery time after oxidation, and the ability for hydrophobic analytes to adsorb onto the PDMS surface (Zhou, Ellis et al. 2010). Because PDMS is by far the dominant material used for microfluidics, many PDMS modification techniques have been investigated to combat these issues (Zhou, Ellis et al. 2010, Zhou, Khodakov et al. 2012). This section will focus on the method of silanization, or the coating of a surface with functional silane molecules.

Silanization is a widely used technique that is used to create a self-assembled monolayer (SAM) using alkoxy- or chlorosilanes with functional head groups to achieve desirable surface properties. This technique can be performed on many substrates if they have surface hydroxyl groups, which once oxidized, will react with alkoxysilanes to create covalent Si-O-Si bonds. PDMS was successfully treated *in situ* with a PEG-silane to prevent non-specific protein adsorption by flowing a mixture of $H_2O/H_2O_2/HCl$ to oxidize the microchannel and incubating with 2-[methoxy-(polyethylenoxy)propyl]trimethoxysilane (Sui, Wang et al. 2006). This technique showed long term stability with the water contact angle (WCA) stabilizing at 40° after 2-3 days. A microfluidic assay was developed by patterning 3-aminopropyltrimethoxysilane (APTMS) to obtain patterned amine functionalities in a microchannel (Seguin, McLachlan et al. 2010). To accomplish this, PDMS was plasma-oxidized and coated with an aluminum film to preserve the hydrophilic surface. The aluminum was etched away and the surface was treated with APTMS dissolved in methanol. The water contact angle of the APTMS modified PDMS surface was 63° compared to 107° for native PDMS (Seguin, McLachlan et al. 2010).

Due to the tendency of zebrafish sperm cells to adhere to PDMS and glass after they become immotile, a PEG-silane (2-[methoxy-(polyethylenoxy)propyl]-trimethoxysilane) has been grafted onto the microchannel of the device to prevent non-specific adsorption. This will be accomplished by using a modified version of the procedure outlined by Sui et al. However, instead of using wet-chemical oxidation to create binding sites for the silane, plasma oxidation will be used. The details of this technique will be discussed further in Sections 2.1 and 2.3.

1.10 Significance

The LOC device proposed will serve as a simple and reproducible means to perform quality evaluation on zebrafish sperm samples. This device has the potential to aid in the standardization of gamete quality analysis and gamete biology research for zebrafish sperm by reducing the human error in experiments involving investigation of sperm motility. It will also enable studies of motility duration and osmolality curves, serving as a LOC device with greater throughput and capability than the few other devices reported (Park, Egnatchik et al. 2012, Scherr, Knapp et al. 2015). Overall, the standardization of gamete quality analysis techniques across research laboratories will offer researchers the capability to reduce the ambiguity in data generated from studies involving zebrafish sperm (Yang and Tiersch 2009). The basic design of this device will be applicable to any aquatic, externally fertilizing freshwater species through proper scaling of the design, flow rates, and activation environments.

CHAPTER 2: MICROFLUIDIC DEVICE FOR MOTILITY AND OSMOLALITY ANALYSIS OF ZEBRAFISH SPERM

2.1 Objectives

The objectives of this study were to design and fabricate a microfluidic device with the capabilities to: (1) standardize the method of activation for zebrafish sperm so that all cells in a sample are subjected to the conditions needed to activate in a reproducible way, (2) reproducibly enable motility analysis of the activated sample within 5 s after activation without the interference of bulk fluid flow, and (3) facilitate the generation of activation curves by relating osmolality of the sample solution to percent motility at the time when motility analysis was performed. This device will be used to evaluate the motility of fresh *Danio rerio* sperm after activation in terms of percent motility, motility duration, and osmolality of the cell suspension.

2.2 Introduction

Zebrafish (*Danio* species) have become a popular vertebrate model organism due to their optically clear embryos, high fecundity, short generation interval, and the ability to apply efficient invertebrate-style genetics to vertebrate-specific questions (Dooley and Zon 2000, Lieschke and Currie 2007). This popularity has resulted in the generation of several thousand mutant, transgenic, and wild-type zebrafish lines, however maintaining all of these lines as live fish is expensive, inefficient, and unrealistic (Hagedorn, Ricker et al. 2009). As a solution to these complications, cryopreservation can be utilized to reduce the cost of maintaining myriad live strains, and provide the opportunities for lines to be shared among research laboratories on demand (Tiersch, Yang et al. 2007). Pre-freeze and post-thaw quality analysis is an essential step in determining the proper techniques for cryopreservation.

Sperm motility analysis is the current standard for determining the quality of a sample. However, motility analysis of zebrafish sperm is difficult due to the small semen yield for each fish (1-2 μL), small sperm size, and short motility duration (10-15 s peak burst motility) (Wolenski and Hart 1987, Wilson-Leedy and Ingermann 2007). For an externally fertilizing,

freshwater aquatic species such as zebrafish, motility is initiated by introducing the sperm to a hypoosmotic environment. The shift in osmolality causes the initially dormant sperm to become active. The process by which this sudden activation happens has been thoroughly studied (Cosson 2004, Wilson-Leedy and Ingermann 2007, Wilson-Leedy, Kanuga et al. 2009, Scherr, Knapp et al. 2015), however little is still known about the exact cascade of events this shift in osmolality induces in freshwater fish. Motility analysis is performed by first activating the sperm, typically by manual dilution and hand mixing (see Figure 5 in Section 1.3), and motility is estimated either visually or through the use of computer assisted sperm analysis (CASA) systems (Wilson-Leedy and Ingermann 2007). The ~10 s time lag between activation and analysis, along with inconsistencies in activation due to human error, are limitations in measuring peak motility of fish sperm, which may result in error-prone evaluation of sperm sample quality. Therefore, there is a need for a platform that enables the rapid mixing and activation of small volumes of zebrafish sperm cells and time sensitive motility analysis.

Microfluidic platforms have the ability to shorten analysis times and reduce the volumes of samples needed. Lab-on-a-chip technology has been used in gamete based studies to sort and orient sperm using hydrostatic pressure (Seo, Agca et al. 2007). The utility of microfluidics has also been demonstrated in Murine in vitro fertilization (IVF) technology, where there was an increase in fertilization rate of 10-27% in microchannels versus center-well dishes for concentrations of sperm in the range of $2x10^4$-$8x10^4$ cells/mL (Suh, Zhu et al. 2006). Furthermore, microfluidic devices provide a geometrically constrained microenvironment that is similar to the in vivo microenvironment, creating an ideal setting to study the dynamics of sperm and fluid flow interactions (Beebe, Mensing et al. 2002). To date, only two microfluidic devices have been developed specifically for the activation of zebrafish sperm cells for motility assessment, so this field is relatively open for exploration and new contributions (Park, Egnatchik et al. 2012, Scherr, Knapp et al. 2015) (Table 1).

Table 1: A comparison of previous microfluidic devices used to activate zebrafish sperm.

Micromixer	Flow Driving Method	Flow Cessation Method	Facilitation of CASA Analysis	Flow Cessation Time (Δt_{fs})	Percent Motility	Reference
Staggered Herringbone	Syringe pump	Turn off syringe pump	Hamilton-Thorne 2X-CEL CASA slide (Hamilton Thorne Biosciences, Beverly, MA)	≥10 s	56 ± 4%	(Park, Egnatchik et al. 2012)
Sequential Logarithmic Mixing Apparatus	Syringe pump	Solenoid valves	On-chip viewing chamber	5-8 s	63 ± 8%	(Scherr, Knapp et al. 2015)

2.3 Device Design Considerations

The general purpose of this microfluidic device is to aid in the standardization of zebrafish sperm quality analysis. This standardization can be achieved by setting in place design constraints that satisfy the essential needs required to ensure that the conditions experienced by the cells during zebrafish sperm motility analysis are reproducible.

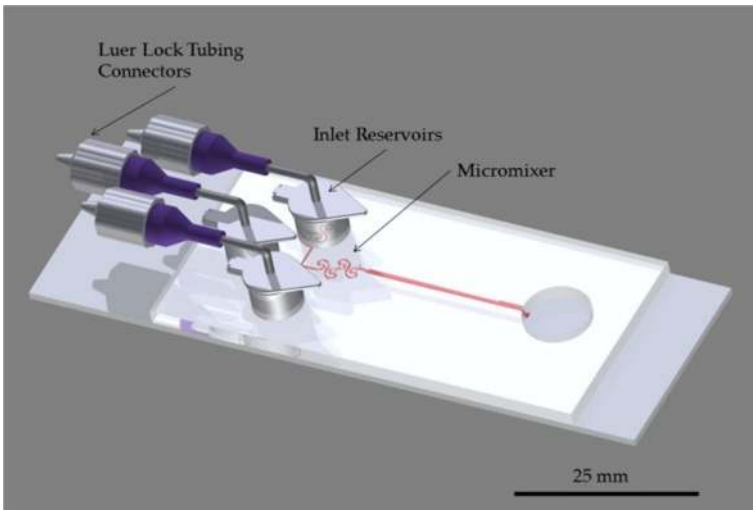

FIGURE 9: Design of sperm analysis chip using the SeLMA micromixer.

The first was to standardize the method of activation for zebrafish sperm so that all cells in a sample are subjected to the conditions needed to activate in a reproducible way. The next constraint was to reproducibly enable motility analysis of the activated sample within 5 s after activation without the interference of bulk fluid flow. Performing analysis within the first 5 s of after activation ensured that the data was consistently collected during the burst motility phase

of activation, removing variation in motility due to time lag typically associated with manual activation methods (Section 1.3). The final constraint was to facilitate the generation of activation curves by relating the osmolality of the sample solution to percent motility at the time when motility analysis was performed.

By using the design constraints listed above, the device shown in Figure 9 was fabricated. To address the first objective, the design incorporated a passive micromixer. Two micromixers were investigated: the staggered herringbone mixer (SHM) and the sequential logarithmic mixing apparatus (SeLMA). The staggered herringbone mixer and SeLMA have each proved to be viable options for zebrafish sperm cell activation (Park, Egnatchik et al. 2012, Scherr 2014). However, careful consideration must be made before choosing the best fit for the device proposed. Because passive micromixers rely on geometric features in the microchannels to facilitate mixing, it is useful to consider the mechanical stresses on the cell caused by these features. A model was produced that tracks the strain rate experienced by particles moving through the SHM and SeLMA (Figure 10) (Scherr 2014). The model predicted that the herringbone mixer subjected cells to a consistently low strain rate (< 300 /s) with

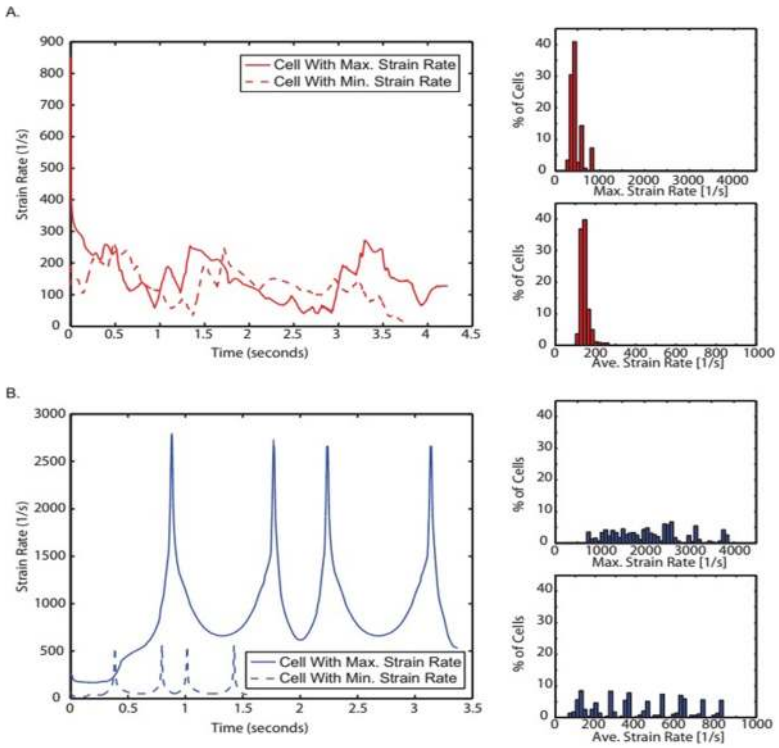

FIGURE 10: The minimum (dashed line) and maximum (solid line) modeled strain rates experienced by a particle as it moves through a microchannel in A) the Herringbone micromixer and B) the SeLMA micromixer (Scherr 2014).

similar maximum and minimum values for strain. However, the predicted strain rates experienced in SeLMA were dynamic and, at the maximums (~2800 /s), approximately an order of magnitude higher than those experienced in the herringbone mixer. This introduces concern for sperm cell integrity, and calls for further investigation in order to validate this model. One option to alleviate this issue and decrease strain rate is to widen the constricted regions of SeLMA from 20 μm to 200 μm. While this modification is likely to reduce mixing efficiency, it may serve as an option if the device retains the ability to activate sperm samples effectively.

To address the second design constraint, the device needed to be able to halt flow in under 5 s after activation in order to be accurately analyzed during the peak burst motility phase of activation. As discussed in Section 1.6, using a syringe pump to drive flow caused an undesirable 5-10 s period of residual flow after the syringe pump was stopped (Park, Egnatchik et al. 2012, Scherr, Knapp et al. 2015). To avoid this, a more simple and equipment-free pumping system was implemented. The system consisted of integrated PCR microcentrifuge tubes at the device inlets, with the caps connected via tubing to a simple one-way pneumatic bulb fabricated from a transfer pipette (8 mL General Purpose Transfer Pipet, Large Bulb, Cat#: 204, Thermo Scientific Samco, San Diego, CA).

The use of PCR microcentrifuge tubes has many benefits. First, they allow for the sample to be directly pipetted into the reservoir tube, rather than pulled into syringes under vacuum, which is easier and reduces the setup time of the device. The use of a syringe pump also requires the use of tubing to transport the sample to the device, which requires a volume of ~200 μL to fill the dead space of the tubing and drive flow through the device. The PCR tube setup only requires ~60 μL of sample to drive flow. Because there is standing fluid in the inlets, the microchannel outlet reservoir has an enlarged 8 mm diameter that is left open to atmosphere, which serves to balance the hydrostatic pressure generated at the inlets. This is done by filling the outlet with enough fluid to match the pressure at the inlets. This design has the capability to

produce static flow by allowing the pressure driving the flow to be removed rapidly. This is done by creating a hole with an approximate diameter of 2 mm in the bulb portion of the pipette, allowing pressure to be applied to the device by hand while the hole is covered. This hole is covered by the finger of the user when the bulb is squeezed, generating pneumatic pressure in the device reservoirs, which drives the sample through the microchannel. To release pressure in the system and halt flow, the bulb and relief hole are released. If it is assumed that the volume of fluid being pushed through the device is equal to the total volume of the device channels, the volume of fluid entering the outlet after one pipette push is less than 0.5 μL. The change in fluid height in the outlet reservoir, and the resultant change in pressure can then be calculated using the equations:

$$h = \frac{V}{\pi r^2} \tag{2}$$

$$P = \rho_f g h \tag{3}$$

Where h is the change in fluid height in the outlet, V is the volume of the fluid, r is the radius of the outlet, P is the pressure, ρ_f is the density of the fluid, and g is the acceleration due to gravity. The change in fluid height was calculated to be less than 10 μm per pipette push, and the resultant change in pressure was under 0.1 N/m^3. This change is pressure is small enough that the fluid does not move back towards the inlets. Evaluation of these design features was accomplished by visually tracking the movement of polystyrene microbeads flowing through the channel under a microscope, and performing particle tracking analysis to assess control of flow in the device.

For the final constraint of facilitating the generation of activation curves that relate osmolality to percent motility, two monolithic floor electrodes were utilized to interrogate the osmolality of the sample solution through impedance spectroscopy. The electrodes were placed such that the fingers protruded into the viewing chamber (Figure 11). This allowed the on-chip measurement of osmolality and percent motility (Section 2.4.7).

As stated above, the purpose of this device was to aid in the standardization of zebrafish sperm quality analysis. Thus, it is advantageous for the device to be reusable. However, as zebrafish sperm transition from motile to immotile, they adhere to the glass slide base. In an effort to prevent sperm cell adhesion in the device, the microchannel surfaces were treated with 2-[methoxy (polyethyleneoxy) 6-9propyl] trimethoxysilane (Gelest, Morrisville, PA). This treatment results in a hydrophilic PEG-grafted microchannel that has been shown in literature to prevent non-specific protein adsorption (Sui, Wang et al. 2006).

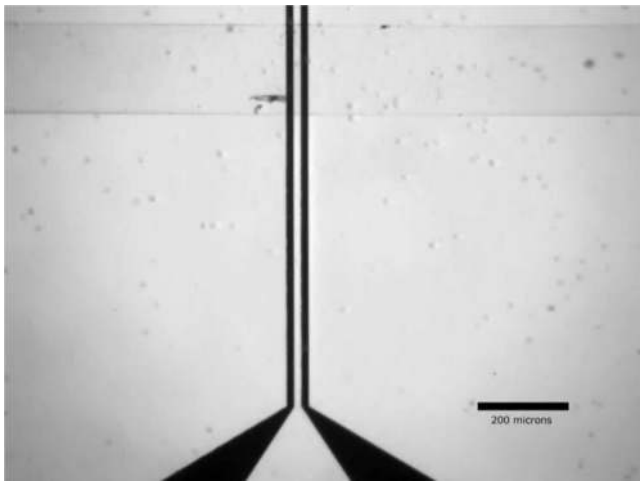

FIGURE 11: Two-prong gold floor electrode used for impedance measurements placed across in the viewing chamber of the microchannel.

The final device consisted of a three-inlet T-channel with an integrated micromixer for the activation of sperm samples (Figure 12). Briefly, the zebrafish sperm sample is loaded into the inlet reservoir, then driven, along with diluent, through the micromixer using pneumatic pressure from the transfer pipette. The activated sperm sample was introduced to the viewing chamber. The flow was stopped, and CASA motility readings were performed while the osmolality of the solution was interrogated by impedance spectroscopy. After CASA completed its protocol, the sample was transported out of the chip and discarded, enabling subsequent analysis of samples.

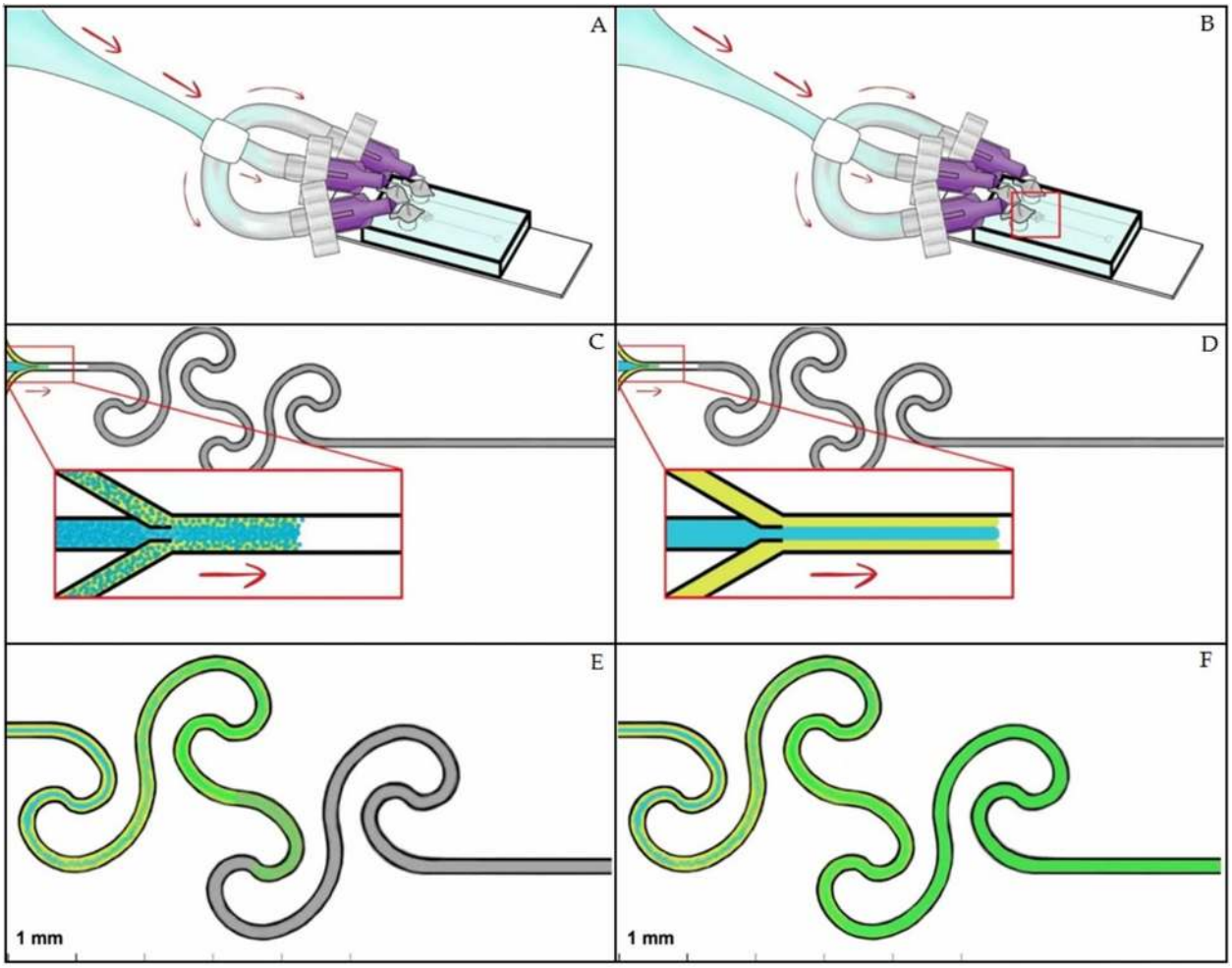

FIGURE 12: Overview of LOC device operation (A-B) As the transfer pipette is squeezed, the inlet reservoirs are pressurized. (C-D) This results in the sample and diluent being pushed through the channel into the micromixer. (E-F) As the fluid passes through the micromixer, the sample and diluent are mixed.

2.4 Materials and Methods

2.4.1 Device Fabrication

AutoCAD (2015 version, San Rafael, CA) was used to create geometries for the microchannel and electrode designs. Silicon master molds were patterned with SU-8 and fabricated using a single step photolithography process. SU-8 2025 (MicroChem Corp., Newton, MA) was utilized to create a negative photoresist mold on a 4 in silicon wafer (Universtiywafer.com, South Boston, MA). Protocols from MicroChem were adapted for the photolithography process (MicroChem). The SU-8 was coated on the silicon wafer using a spin coater (WS-650 Series Spin Processor, Laurell Technologies Corp., North Wales PA) at 3000 rpm for 30 s to achieve a thickness of 40 μm. The wafers were pre-baked on a hot plate at 65 °C for 5 min and then at 95 °C for 15 min with a ramp up of 2 °C/min and gradually cooled down to 25 °C over 2 hrs. Following baking, the wafers and photomask were positioned into a custom exposure system that utilizes a Blak-Ray B-100 series UV lamp (UVP, LLC; Upland, CA), and were exposed to 365 nm UV light with an intensity of approximately 2 mW/cm^2 for 80 s for an effective dose of 160 mJ/cm^2. After exposure, the wafers were baked with the previous ramp up and cool down temperature-time procedure. The wafers were immersed in an SU-8 developer solution (MicroChem Corp., Newton, MA) for 5 min, followed by a fresh developer rinse for 1 min, a last rinse with isopropyl alcohol, and finally dried with compressed nitrogen gas (Ultra High Purity, Airgas, Baton Rouge, LA).

The electrodes were fabricated by the following procedure: An optical mask was purchased from the Advanced Reproductions. Glass slides (2x1 in, Cat#: 3048-002, Gold Seal Plain Glass Microscope Slides, Thermo Scientific, Waltham, MA) were coated with MICROPOSIT S1813 (Dow Chemical, Midland, MI) positive photoresist using a spin-coater at CAMD. The photoresist was spin-coated onto the glass slide at 2000 rpm for 60 s. The spin-coated glass slides were baked on a hot plate at 115 °C for one min. UV exposure through the optical mask

was done at a UV exposure dose of 40 mJ/cm^2 using the Quintel UL7000-OBS Exposure Station (Neutronix Quintel, Morgan Hill, CA). The exposed samples were developed in diluted AZ400K developer (Microchem Corp., Newton, MA) (1:4, AZ 400K:deionized water) for 1 min. Deionized water refers to water passed through a Millipore Synergy® UV Purification System and dispensed at 18.2 MΩ. The samples were rinsed with DI water and dried with nitrogen. The samples were baked on a hot plate at 115 °C for 1 min. After baking, the samples were cleaned in 100% oxygen plasma using the Reactive-ion etching (RIE) at 150 mT at a power of 100 W for 1 min. Then the samples were coated with 10 nm Cr/ 100 nm Au using an e-beam evaporator at the University of Texas at Dallas. Then the samples were immersed in Acetone for the lift-off process of the photoresist, resulting in the microelectrodes on glass slides.

The final device was fabricated using traditional soft lithography processes. Briefly, Sylgard 184 polydimethylsiloxane (Dow Corning, Midland, MI) was poured onto the master wafer at a ratio of 10:1 (base: curing agent). The PDMS was cured in an oven at 65 °C for 90 min and removed from the mold. The inlet access holes were created using a 6-mm Harris Uni-core biopsy punch, and the outlet was made using a 8-mm punch. The PDMS devices were trimmed and irreversibly bonded to a clean glass microscope slide using a Harric Plasma Cleaner, PDC-32G (Harric Plasma, Ithaca, New York) for 30 s at 1.8 W. The plasma-treated channel was subjected to 2-[methoxy(polyethyleneoxy)6-9propyl] trimethoxysilane within 1 min of bonding and left to sit for 15 min. The unreacted silane was removed by flowing deionized water into the

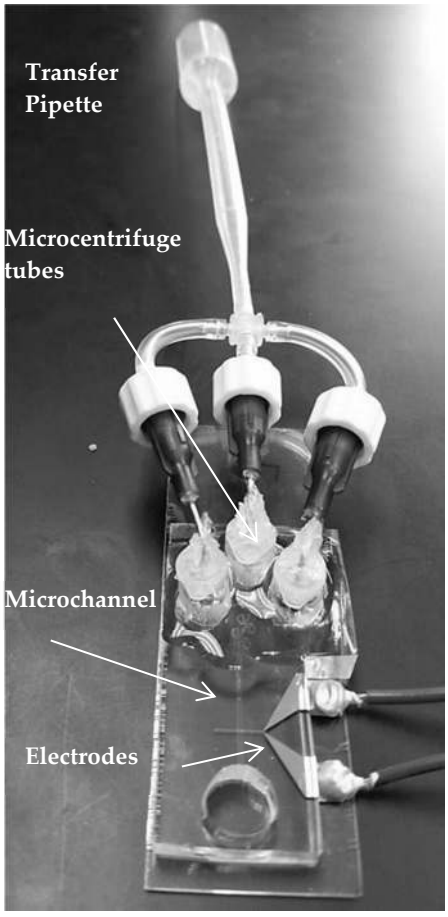

FIGURE 13: Assembled Microfluidic Sperm Analysis Chip.

channel for 5 min and dried by flowing nitrogen gas through the channel until all remaining fluid was evaporated.

To create the inlet reservoirs, microcentrifuge tubes were cut at the junction of the tapered and untapered region, and pneumatic access holes were created by punching through the cap with a sharpened 21g needle (OD 820 μm). The tubes were inserted into the device inlets and the area around the tubes was sealed with PDMS and the chip was baked at 65 °C for 90 min. Blunted 0.5 in, 90° bend 21g needles were inserted into the pneumatic access holes, which were then sealed using clear, waterproof silicon adhesive (P/N: 12045, ITW Consumer, Hartford, Conneticut). The sealant was allowed 24 hrs to cure. The pneumatic connection was created by using a tubing adaptor that connects a lure lock needle to 1/8" tubing by using a female lure lock attachment on one side and a 1/8" tubing barb on the other (MTLL230-1, Nordson Medical, Loveland, CO). The adapter was connected to 1/8" Tygon tubing, which ran to a 4-way barbed tubing connector (4PX230-1, Nordson Medical, Loveland, CO). The pneumatic driver was fabricated out of an 8-mL polypropylene transfer pipette (Samco, Thermo Scientific, Waltham, MA) by creating a hole in the bulb portion of the pipette with an 18g needle (Figure 13).

2.4.2 Flow Rate and Cessation Analysis

As previously discussed, the flow in the device is generated by applying pneumatic pressure to the headspace of the microcentrifuge tubes by compressing the transfer pipette. A small pneumatic regulator (R-7010, Air Logic, Racine, WI) was used to control the amount of pressure applied to the device, allowing the flow rate to be manipulated. Particle tracking velocimetry (PTV) was used to correlate the applied pressure to the flow rate. Because the maximum pressure that the transfer pipette could generate was determined to be approximately 3 psi by observing the pressure gauge of the regulator while squeezing the pipette bulb, the flow rate was analyzed at 1, 2, and 3 psi.

It is imperative that sperm analysis be performed by CASA as soon as possible following activation due to the short motility duration of zebrafish sperm. Measurement of motility using CASA requires static flow conditions so that bulk fluid drift does not influence the results. The device created by Park, Egnatchik et al. (2012) accomplished this by simply turning off the syringe pump as cells entered the viewing chamber. This method required a minimum of 10 s at the lowest flow rate for bulk fluid drift to subside after sperm activation. A 10 s delay cuts into the already short motility duration and inhibits analysis of the sperm during the brief 10-15 s burst motility phase. The device created by Scherr, Knapp et al. (2015) improved upon this design by using solenoid pinch valves to occlude the inlet and outlet tubing to reduce bulk fluid drift. However, this method still required a latent period of 5-8 s after activation for bulk fluid drift to subside enough for measurement by CASA. The current device sought to reduce the time for flow cessation considerably in an effort to ensure that analysis could be carried out within 5 s after sperm activation.

Briefly, 6 μm microparticles (Polysciences, Inc., Warrington, PA) were introduced to the device at 1, 2, and 3 psi. The particles were recorded at 120 frames/s using the MoviePro app (Version 5.2, Depak Sharma) on an iPod 6 (Apple, Cupertino, CA) mounted to the microscope eyepiece. These videos were segmented into image sequences and thresholded using Fiji image processor (Schindelin, Arganda-Carreras et al. 2012). The Mosaic 2D/3D Particle Tracker plugin for Fiji was used to find the trajectory of each particle in the image sequence (Sbalzarini and Koumoutsakos 2005). These trajectories were analyzed to find the particle displacement between each frame, which was divided by the time between each frame to find the velocity. Assuming that the microparticles were moving at the same velocity as the fluid, the flow rate was found by using the equation $Q=VA$, where Q is the flow rate, V is the fluid velocity, and A is the cross sectional area of the microchannel perpendicular to flow.

2.4.3 Sample Handling and Acquisition

Protocols for the use of animals in this study were reviewed and approved by the Louisiana State University Institutional Animal Care and Use Committee (Baton Rouge, LA). Adult Zebrafish (*Danio rerio*) were obtained from the Zebrafish International Resource Center (ZIRC, OR, USA). Fish were maintained within a 638-L recirculating system. Water quality parameters were maintained at 28.5° C (temperature), 8.5 (pH) and 12-h light:12-h dark (photoperiod). Fish were fed to satiation twice daily with a dry food master mix (http://zebrafish.org/ documents/protocols/pdf/Fish_Feeding/Flake_Food/Dry_Food_Recipes2015.pdf, accessed on May 10, 2015) in the morning and artemia (Brine Shrimp Direct, Ogden, Utah) in the afternoon. Additional water quality parameters that were monitored weekly and kept at an acceptable range included: ammonia (0 - 1.0 mg/L), nitrites (0 - 0.8 mg/L) and nitrates (0 - 15 mg/L). For sperm collection, fish were anesthetized with 0.01% MS-222 (Tricaine methanesulfonate, Western Chemical, Inc. Ferndale, WA). Fish were placed ventral side up on a moist sponge and gently stripped. Sperm were collected into a glass capillary tube and mixed with Hanks' balanced salt solution (HBSS, 0.137 M NaCl, 5.4 mM KCl, 1.3 mM CaCl2, 1.0 mM MgSO4, 0.25 mM Na2HPO4, 0.44 mM KH2PO4, 4.2 mM NaHCO3, and 5.55 mM glucose, pH 7.2) at 300 mOsm/kg. Given the limited volume of sperm collectable from Zebrafish (1 to 3 μl), pooled sperm samples from as many as 6 individuals were used.

2.4.4 Comparison of Microfluidic vs. Manual Activation

As previously stated, the general theme of this device was to standardize zebrafish sperm analysis. This requires eliminating the high variability in manual sperm activation. If the activation performance of the micromixer outweighs that of manual activation methods, it will solve a crucial problem with sperm quality analysis and facilitate the standardization of gamete quality analysis procedures. To validate the utility of the device, it was be necessary to compare percent activation over time for multiple trials between manual activation performed by a

trained technician, and micromixer facilitated activation on a microfluidic platform. This validation was carried out by performing motility analysis via CASA on a single sample using manual activation and then analyzing the same sample on-chip.

A commercially available CASA instrument was used (HTM-CEROS, version 14 Build 013, Hamilton Thorne Biosciences, Beverly, Massachusetts, USA). Images were captured (100 frames) at a rate of 60 frames/s. The minimum contrast was 50 and minimum cell size was 2 pixels. The default values when less than 5 cells were motile were set at 4 pixels for cell size and 65 for cell intensity. Briefly, manual activation was performed using by pipetting 1 μL of a sperm sample onto the bottom portion of a Makler® Counting Chamber (Irvine Scientific, Santa Ana, CA), which was diluted with 2 μL of deionized water. The sperm sample was mixed with the tip of the pipette, and the top of the Makler® Counting Chamber was placed on top to create a monolayer of cells. The chamber was placed on the microscope and analyzed via CASA. On-chip activation was performed by first placing the device on the microscope and adjusting the focus on the viewing chamber. Sperm sample (60 μL) was pipetted into the center inlet of the device, and 60 μL of deionized water into each side inlet. The pneumatic bulb was squeezed and the sperm and deionized water were driven through the micromixer, activating the sample. The sperm were transported directly into the viewing chamber, where flow was halted, and the sample was analyzed using CASA. Due to the small volume of the chip (<0.5 uL), the same 60 uL sample was used for all trials.

2.4.5 Generation of Activation Curve

The assessment of sample osmolality within the microchannel would facilitate the generation of sperm activation curves, used to determine the optimal osmolality at which the sperm in the sample activate. One primary reason to determine osmolality on-chip is that different dilutions can be created by adjusting the flow between sperm and diluent, or by using HBSS in diluent sample inlets. This information will aid in discovering the proper protocols for sperm

activation, and give insight to the physiological mechanisms by which the sperm transition from non-motile to motile. To create an activation curve, the percent activation and motility duration of zebrafish sperm samples were assessed using CASA. The samples were analyzed at four different osmolalities ranging from 100-300 mOsm, increasing at 50 mOsm increments. The sperm were activated using on-chip activation methods. The final osmolality of the sample was manipulated by using HBSS dilutions in the diluent reservoirs. To determine the correct osmolality of the diluent needed to achieve the desired final osmolality, samples of HBSS300 were mixed in a 2:1 ratio (Diluent:HBSS300) with HBSS dilutions ranging from 16-305 mOsm. The final osmolality was determined by using a freezing point depression osmometer (Table 3). The osmolality of the sample was measured via impedance spectroscopy using the on-chip electrode by interrogating the sample while still in the channel.

2.5 Results and Discussion

2.5.1 Surface Modification using PEG-Silane

Previous reports have shown the silanization of PDMS using 2-[methoxy (polyethyleneoxy)6-9propyl]trimethoxysilane (Sui, Wang et al. 2006), however the effects on glass are currently unreported. Contact angle experiments were employed to investigate the surface properties of PEG-silane treated glass. Clean glass slides were treated using the same procedure used on the micro-device, and the water contact angle was analyzed after a treatment time of 5 min and 15 min. The water contact angle of the treated glass decreased from 24.10 ± 0.76° of native glass to 13.68 ± 3.09° after a treatment time of 5 min, and decreased further to 6.68 ± 1.74° after a treatment time of 15 min. The decrease in water contact angle shows the hydrophobicity of the glass decreased after treatment with the silane, indicating that a hydrophilic layer was formed.

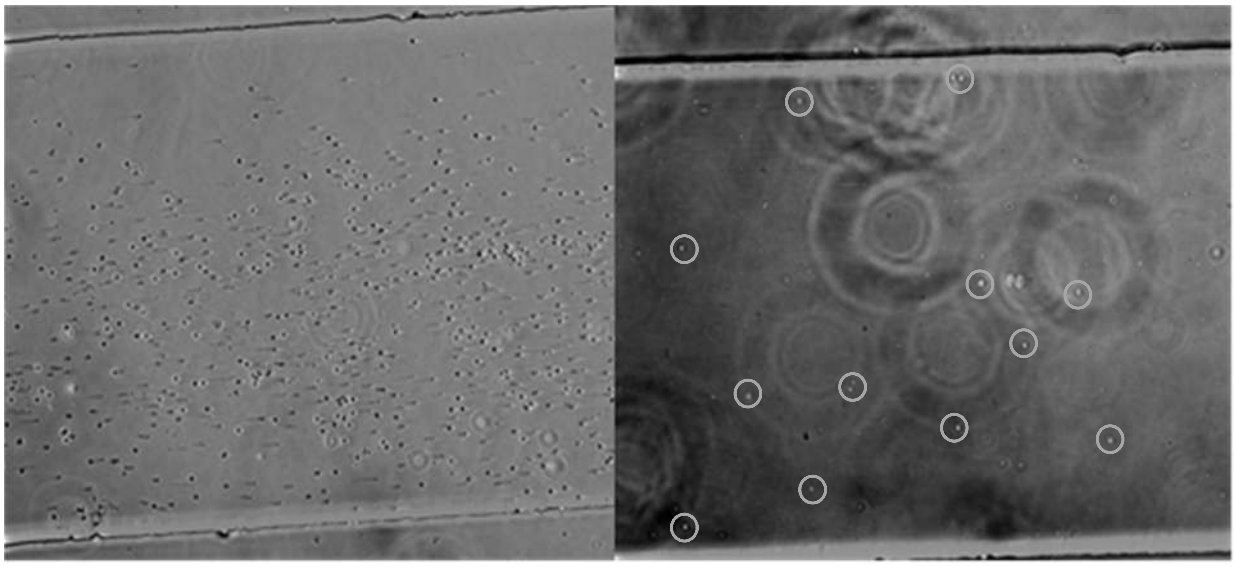

FIGURE 14: An untreated microchannel (Left) and a PEG-grafted microchannel (Right) after a sample of zebrafish sperm has been introduced to the device. Sperm cells in the treated device are indicated, so as not to be confused with camera artifacts (Magnification 100x)

To test the cell-repelling characteristics of the PEG-grafted microchannels, a side-by-side comparison of treated and non-treated microchannels was performed. The treated devices were fabricated using the methods in Section 2.3.2. To perform the experiment, a zebrafish sperm sample with a concentration of approximately $1x10^8$ cells/ml was introduced into the channel of treated and non-treated devices. As shown in Figure 14, there was an increase in cell adhesion for the untreated device compared to the treated devices with more 500 adhered cells in the un-treated device and an average of 12 ± 3 cells adhered in the treated devices. This results indicates treating the microchannel with the PEG-silane reduced the adhesion of zebrafish sperm and was used in all subsequent devices tested.

2.5.2 Flow Rate and Cessation Analysis

The approximate flow rate of the device at 1, 2, and 3 PSI was determined by tracking tracer beads moving through the device as flow was initiated and then ceased. An example of the typical flow rate profile at 2 PSI is shown in Figure 15. As expected, when pneumatic pressure is applied to the device, there is a sharp increase in the flow rate, which then levels off. As

the pressure is removed, there is a rapid decrease in flow rate, indicated by the region labeled $\Delta t_{FC,}$ (time required for flow cessation), from approximately 5 μL/min to 0 μL/min over a period of ~0.6 s (Figure 15).

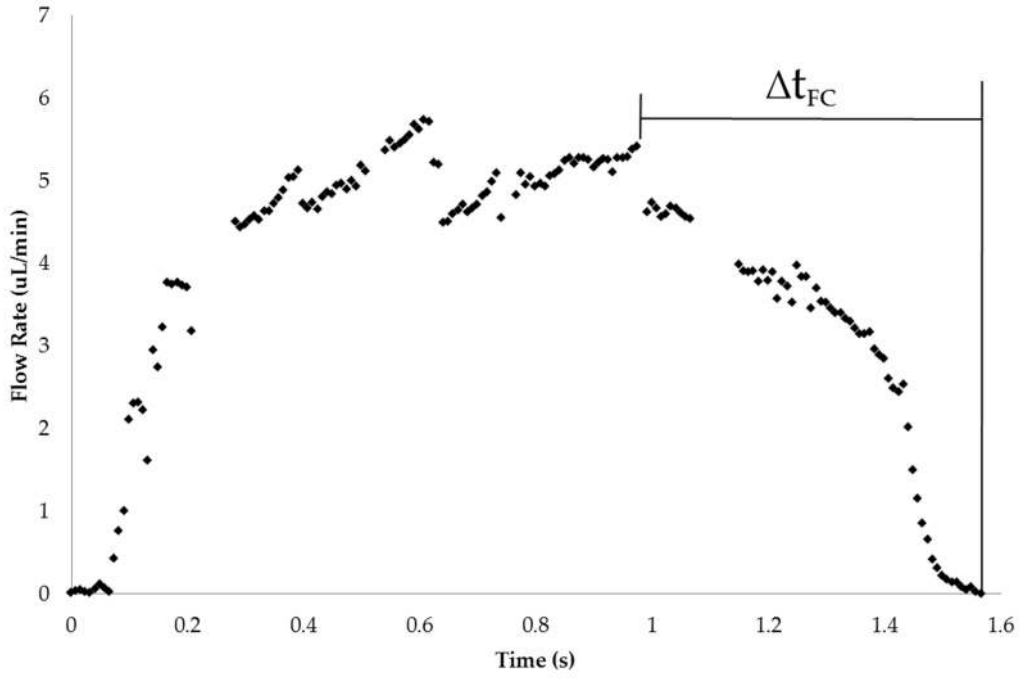

FIGURE 15: A flow rate profile over time for 2PSI as measured using PTV.

The average maximum flow rate was determined by averaging the peak velocities for each pressure. 1 PSI showed the lowest flow rate, with 3.4 ± 0.8 μL/min. There was no significant difference between the flow rates at 2 PSI (8.1 ± 1.7 μL/min) and 3 PSI (9 ± 2.2 μL/min) ($P<0.05$) (Figure 16). The flow rate at 1PSI was statistically different from the flow rates at 2 and 3 PSI ($P<0.05$). This data was expected, because as the pressure increases, the fluid should be pushed though the channel at a greater rate. The Flow cessation at each pressure was determined as the time taken for bulk fluid drift to stop after the pneumatic bulb was released. At 1 psi, bulk fluid flow subsided after 0.31 ± 0.21 s, and at 3 psi, flow cessation was achieved in 0.68 ± 0.22 s. There was no significant difference between the flow cessation times at any of the pressures ($P<0.05$). This represents an improvement over the previous devices reported, which re-

required 5-10 s to achieve flow cessation (Park, Egnatchik et al. 2012, Scherr, Knapp et al. 2015). Halting flow rapidly in the microdevice enables the user to analyze zebrafish sperm quality directly after activation, thus insuring that analysis was performed during the initial 10-15 s burst motility phase of zebrafish sperm activation.

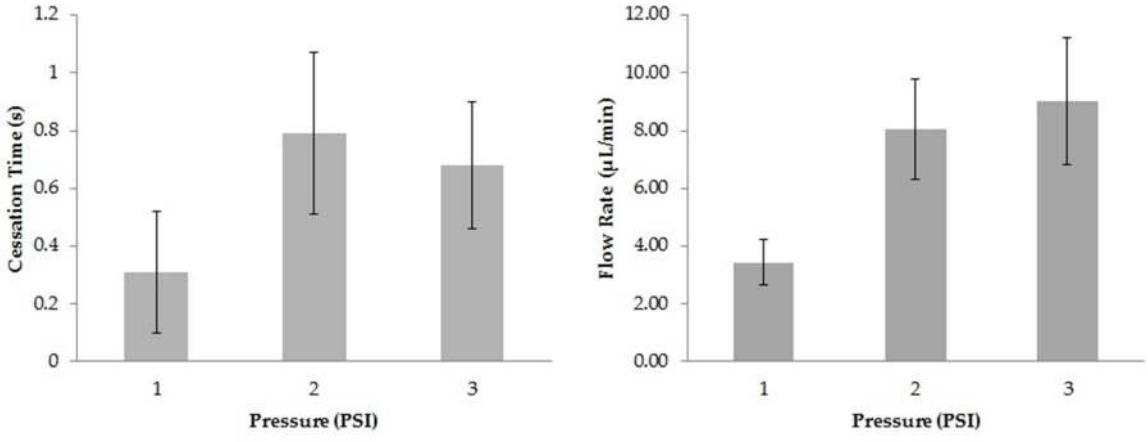

FIGURE 16: (Right) Flow cessation time and (Left) Maximum Flow Rate for pneumatically driven microfluidic chip. (n=3)

2.5.3 Micromixer Selection

To evaluate the mixing efficiency of the SeLMA micromixer compared to that of the Herringbone micromixer, fluorescence was quantified as deionized water and fluorescein were passed through the micromixers. For both devices 50 μM of sodium fluorescein in water (Sigma-Aldrich, St. Louis, MO) was pipetted into the center inlet, while deionized water was put into the two outer inlets, and mixing was analyzed at 1, 2, and 3 psi. The microchannels were imaged at the inlet and outlet using an inverted fluorescent microscope (Eclipse, Nikon Instruments Inc. Melville, NY, USA) with a 10-x objective lens and digital camera (CoolSnapFX Photometrics, Tucson, AZ, USA), and analyzed in Metamorph Software (Universal Imaging, Corp., West Chester, PA, USA). To determine mixing efficiency, a linescan was taken across the channel at each point of interest (Figure 17) and the intensity of the fluorescence was recorded. Mixing efficiency was calculated using Equation 4:

$$Mixing\ Efficieny = \left(1 - \frac{\sqrt{\frac{1}{N}\sum_{i=1}^{N}(I_i - I^{perf.mix})^2}}{\sqrt{\frac{1}{N}\sum_{i=1}^{N}(I^0 - I^{perf.mix})^2}}\right) \times 100\% \quad (4)$$

where N is the total number of pixels, I_i is the intensity recorded at pixel i at a specific location, I^0 is the intensity without mixing or diffusion, and $I^{perf.mix}$ is the intensity of a perfectly mixed solution (Johnson, Ross et al. 2002).

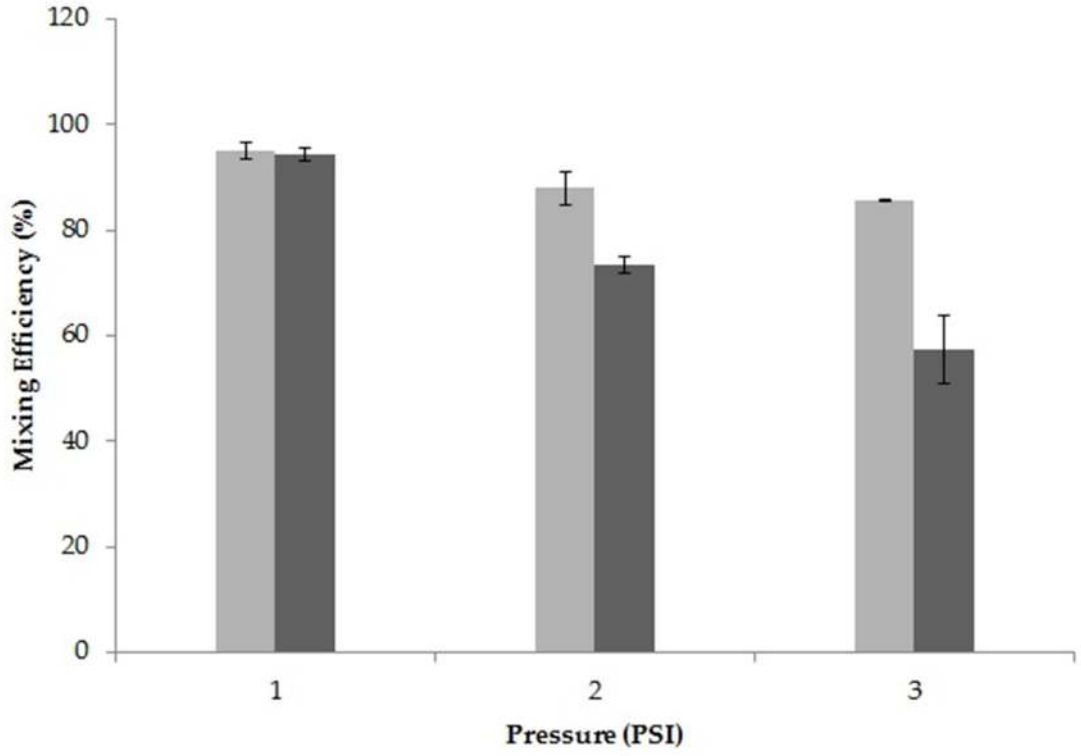

Figure 17: The mixing efficiencies for the Constricted SeLMA (grey) micromixer and the Non-Constricted SeLMA (dark grey) micromixer in relation to the pressure applied to the microdevice to drive flow. Mixing efficiencies for each pressure were calculated by comparing the standard deviation of the intensity values across the channel to the standard deviation of the intensity across a perfectly mixed sample (n=3)

Due to the increase in fabrication time and difficulty associated with multilayer lithography, and the tendency for sperm cells to become caught in the herringbone features, the herringbone micromixer was eliminated. Non-Constricted SeLMA increased in mixing efficien-

cy from 57 ± 6% to 94 ± 1% as the pressure driving flow was decreased from 3 to 1 PSI. Both micromixers showed the highest mixing efficiency at 1 PSI, with 95 ± 2% for the Constricted SeLMA micromixer and 94 ± 1% for Non-Constricted SeLMA micromixer. This was an expected result because mixing is dominated by diffusion at the lower flow rates tested. The mixing efficiency of Constricted SeLMA was statistically higher than Non-Constricted SeLMA at 2 and 3 PSI (Figure 17, $P < 0.05$, n=3). However, due to the tendency of aggregate sperm cells to block the constrictions in Constricted SeLMA, Non-Constricted SeLMA was selected to be incorporated into the final device design.

2.5.4 Analysis of Zebrafish Sperm Activation

Sperm cells at a concentration of $1.0x10^8$ cells/mL in HBSS300 were activated on-chip within 1 hr of stripping and motility was investigated at osmolalities of 100-300 mOsm. This narrow range was chosen because the lowest osmolality that can be generated in a 3-inlet microfluidic device without prematurely activating the sample was 100 mOsm, where the cell suspension is at 300 mOsm and the adjacent diluent channels could be at a minimum of zero osmolality. Approximately 75 μL of sperm sample was loaded into the center inlet of the channel, and equal amounts of deionized water were pipetted into the side inlets. All tests were run

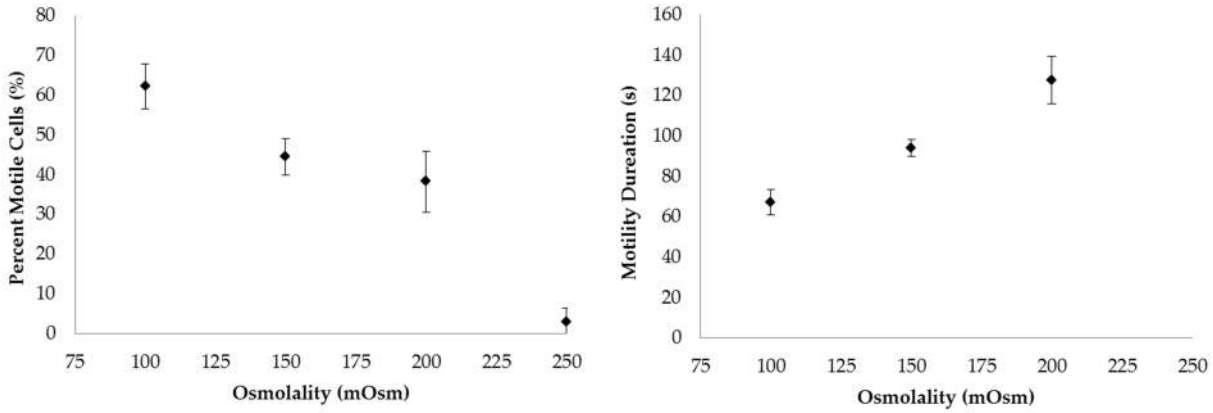

FIGURE 18: Zebrafish Sperm Activation Curve: The motility (left) and the motility duration (right) of zebrafish sperm activated in 4 osmolalities of HBSS. (n=3)

at 3 PSI to give an approximate initial flow rate of 10 μL/min (described in Section 2.3.2). As expected, the percent of motile sperm cells decreased as the osmolality of the final solution was increased (Figure 18). As the osmolality was increased from 100 mOsm to 200 mOsm, the progressive motility decreased from 62 ± 6% to 38 ± 8%. At 250 mOsm, the motility dropped to 3%, which was consistent with previous reports on zebrafish sperm motility (Yang, Carmichael et al. 2007). The increase in the osmotic pressure as the final osmolality of the cell solution increased resulted in a decrease in the duration of cell motility. The swimming duration decreased from 128 ± 12 s to 67 ± 6 s as the final osmolality increased from 100 mOsm to 200 mOsm. This result from the microfluidic format was also consistent with previous reports accomplished via hand mixing (Yang, Carmichael et al. 2007).

2.5.5 Comparison of Manual and Microfluidic Sperm Activation

The activation of zebrafish sperm by hand mixing was compared with on-chip activation using the Non-Constricted SeLMA micromixer device. All tests were carried out until the progressive motility of the sample had reached <1%. In an effort to assess the overall potential of the chip in replacing traditional manual methods, the manual activation was done using a 4:1 dilution in order to increase the activation potential of the sperm. This is in contrast to the resultant 2:1 dilution generated by the microfluidic device. Manual activation (Figure 19) resulted in an initial motility of 58 ± 10%, which then decreased to <1% over 70 s, while on-chip activation had an initial motility of 63 ± 2%, and showed a stable decrease in motility over 140 s. However, initial motility analysis was performed ~10 s after activation for all manual tests due to the time lag associated with this method (Figure 19). There was no significant difference between the percent motility at 10 s for either activation method (n = 3, $p < 0.05$). Due to the difference in dilution ratio, and thus motility duration, comparing data beyond 10 s may not yield relevant results. There was also a higher standard deviation throughout the manual acti-

vation trials, indicating that improper mixing may have resulted in cells becoming active after initial mixing due to diffusion.

In addition to the 4:1 manual dilution study described above, a 2:1 hand dilution was performed to be more consistent with the microfluidic 2:1 dilution ratio (Figure 20). On-chip activation resulted in an initial motility of 66 ± 6%, while manual activation had an initial motility duration of 49 ± 8%. When compared to the manual 4:1 activation, the manual 2:1 activation resulted in a more gradual decrease in motility over time. The percent motility in the 4:1 test

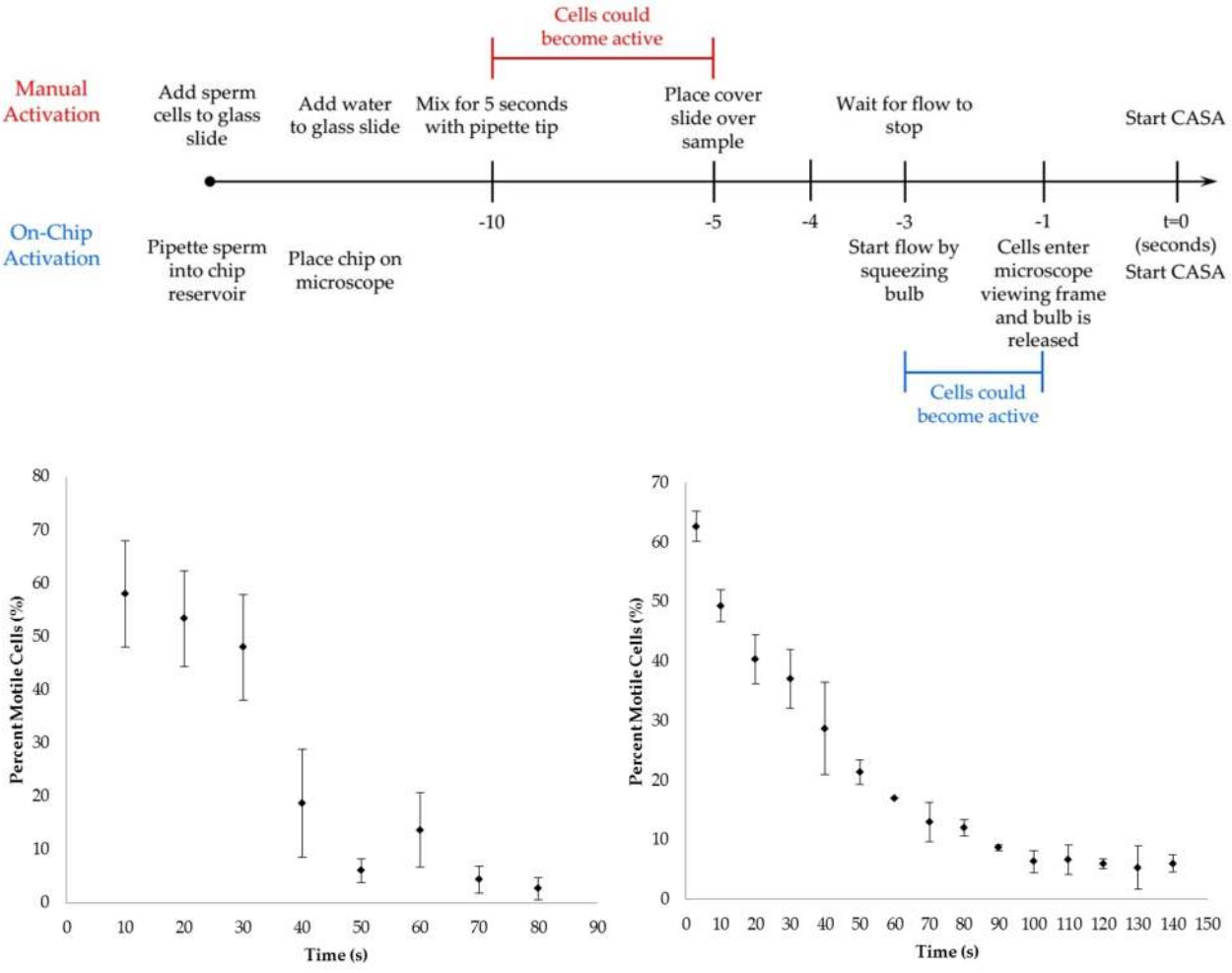

FIGURE 19: (Top) A time line comparing manual to on chip activation. (Left) Manual zebrafish sperm cell activation using a standard 4:1 dilution ratio and (Right) the 2:1 on-chip zebrafish sperm activation

decreased from 48 ± 10% to 19 ±10% between 30 and 40 s, a minimum drop of 9%. This is an expected result, since a higher dilution, and thus a lower osmolality, would result in a faster decrease in motility (Yang, Carmichael et al. 2007).

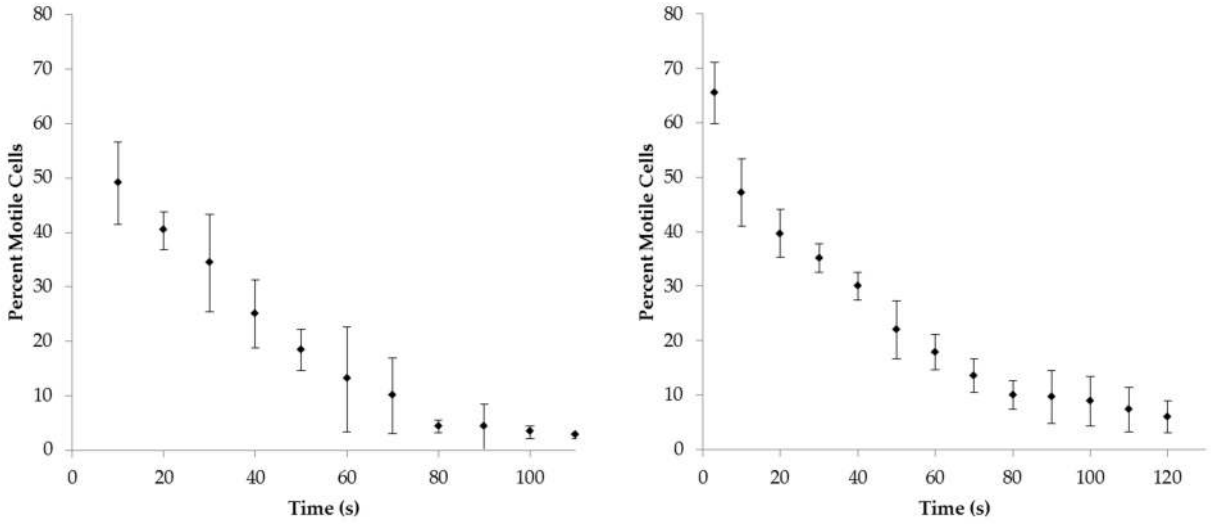

FIGURE 20: Motility over time for (Left) Manual zebrafish sperm activation using 2:1 dilution ratio and (Right) on-chip zebrafish sperm activation using a 2:1 dilution ratio. Due to the time lag associated with manual activation, the time points for that experiment start at t=10.

To compare the on-chip activation data to the manual activation data in terms of statistical significance and variance, a Student's T-Test was performed ($p < 0.05$). Due to the latency period associated with manual activation, the motility was only compared for time points after 10 s. Significance was only found at 80 s (P = 0.014) between the manual activation and on-chip activation (Figure 21). This can be attributed to the higher standard deviation of the manual activation, however an F Test revealed that the only time points with a significant difference between the standard deviations of the two methods were at 30 (P = 0.020), 60 (P = 0.034), 110 s (P=0.016). Because this variability is seen in both instances of manual activation, it is a likely indicator that the hand mixing involved in manual activation is less effective than the on-chip

mixer at providing cells that have the potential to become motile with the appropriate conditions needed to activate.

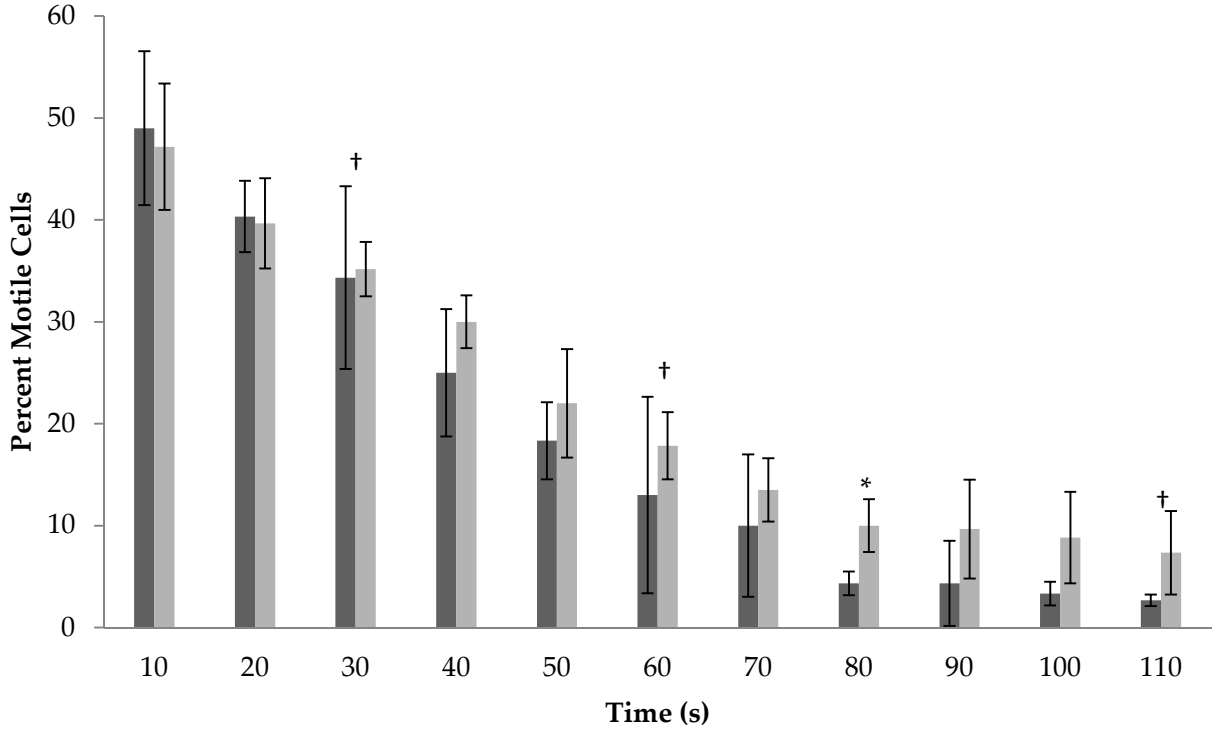

Figure 21: Statistical Analysis of manual (black bars, α=0.05, n=3) and on-chip (grey bars, α=0.05, n=6) activation of zebrafish sperm over time. * Indicates Significance. † Indicates Unequal Variance

2.5.6 Generation of Standard Curve for Osmolality Measurement

As discussed in Chapter 1, impedance spectroscopy can be used to characterize the resistance and capacitance of samples by applying an AC electrical input and measuring the magnitude (resistive) and phase (reactive) components of the resulting signal. An initial analysis of impedance signals as a function of HBSS osmolality was performed by measuring HBSS in the microfluidic device via the on-chip microelectrodes, which was connected to a 660B Electrochemical Analyzer (CHI Instruments Inc., Austin, TX). To determine the optimal frequency at which to interrogate a sample, a bode plot ranging from 1-100,000 Hz was performed on each sample in a seventeen-part dilution ranging from 16-306 mOsm was created.

As frequency increased, there was a greater distinction in the magnitude and phase angle for each osmolality. Thus, it was decided to interrogate the sample at 100,000 Hz. This data can be found in the Appendix. To create a standard curve, impedance analysis was performed on the same seventeen-part dilution of HBSS ranging from 16 to 305 mOsm. The solution was interrogated at $9.668x10^4$ Hz with an amplitude of 0.01 V. The phase angle of the impedance decreased from -11.6°± 0° to -23.57°± 0.05° as the osmolality of the solution increased from 16 mOsm to 305 mOsm (Figure 22). The magnitude of the impedance decreased from 57703 ± 61 Ω to 5127 ± 15 Ω as the osmolality of the solution increased, albeit in a non-linear fashion (Figure 23). This is expected, because the conductivity of the solution should increase (thus decreasing the resistance) with the concentration of ions. There was a very low variability between all tests (<1° and <100 Ω). However, due to small variations between electrodes it should be noted that a standard curve must be created for each device to ensure accuracy.

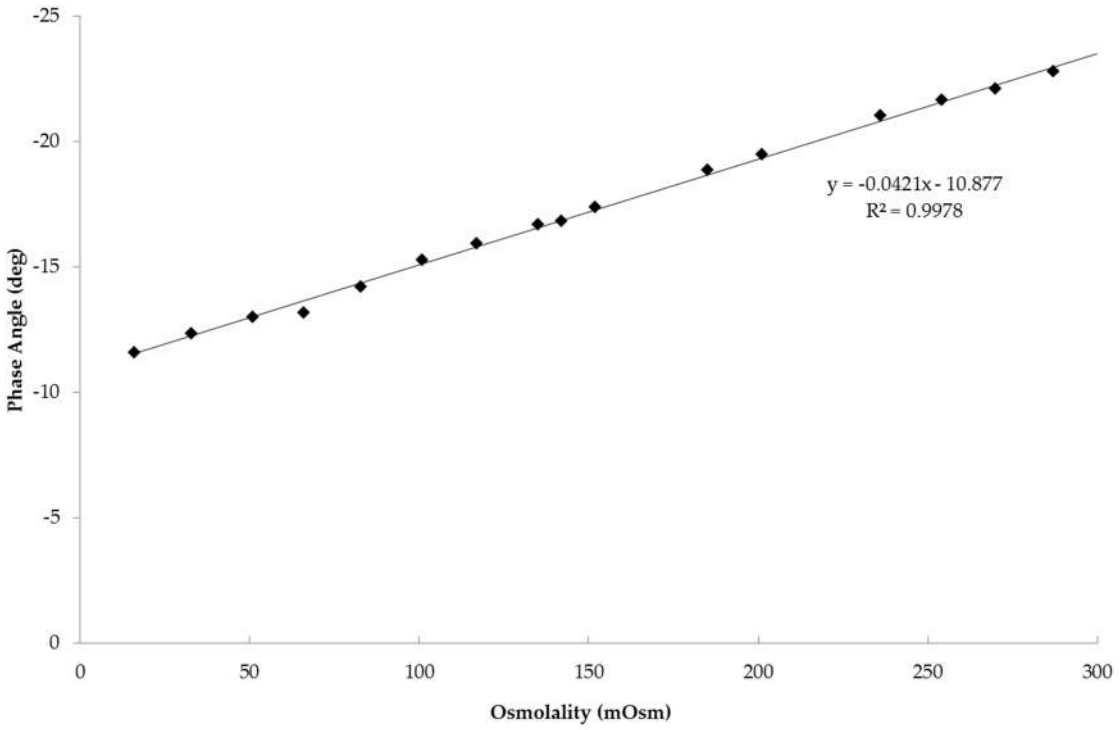

FIGURE 22: Standard Curve for Osmolality Determination of HBSS using the phase angle component of Impedance Spectroscopy. Each point represents the mean ± S.D. of measurements from three samples.

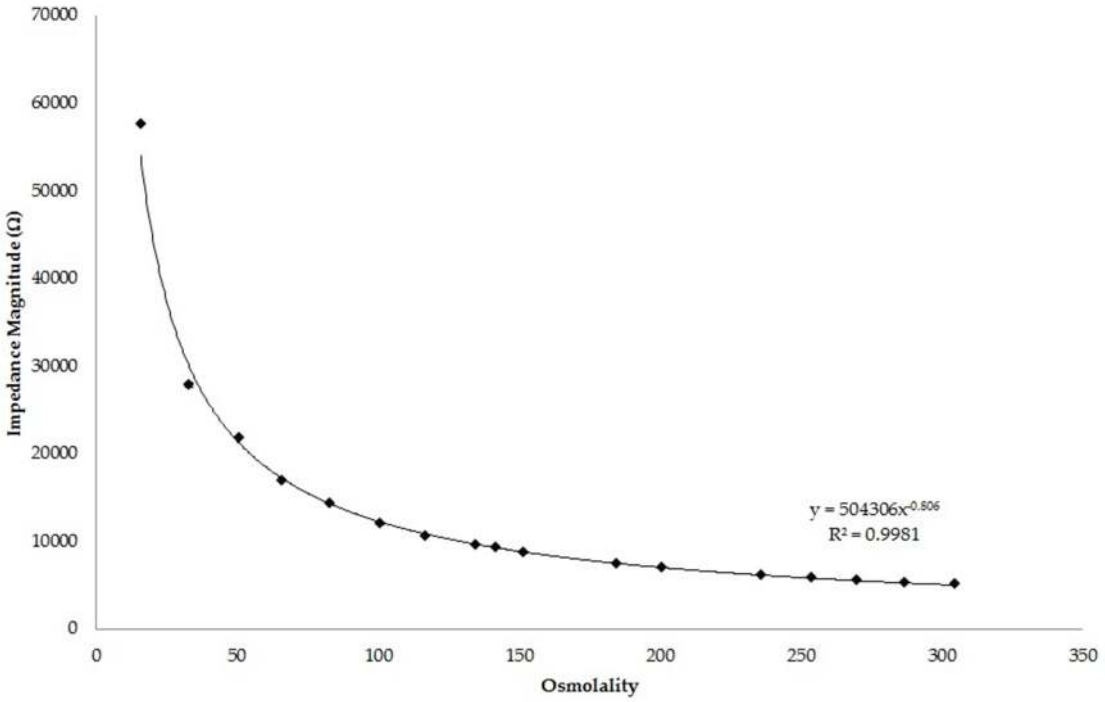

Figure 23: The standard curve for determining the osmolality of a solution by measuring the magnitude of the impedance.

2.5.7 Osmolality Determination of Sperm Sample

The osmolality of a sperm cell solution at a concentration of $1.0x10^8$ cells/mL was interrogated using Impedance Spectroscopy as the osmolality of the solution was increased from 100 to 300 mOsm, increasing at 50 mOsm increments. Both the magnitude and phase angle of the impedance were investigated. After the cells were introduced into the channel, it became apparent that the phase angle component of the impedance no longer correlated to the osmolality (Figure 24). There was no significance between the phase angles at 100 mOsm, but all other points showed significance. This indicated that there was no correlation between the standard curve and the measurements taken with zebrafish sperm in the microchannel (Figure 25).

To determine if the interference caused by zebrafish sperm on the phase angle of the impedance was dependent on the sperm cell concentration, impedance measurements of zebrafish sperm in HBSS at osmolalities of 100, 200, and 300 mOsm were taken at cell concentrations of $1.4x10^8$, $1.05x10^8$, and $7x10^7$ cells/mL (Figure 24). There was no definite trend in phase angle as

the cell concentration was decreased, and all values were statistically different from the standard curve.

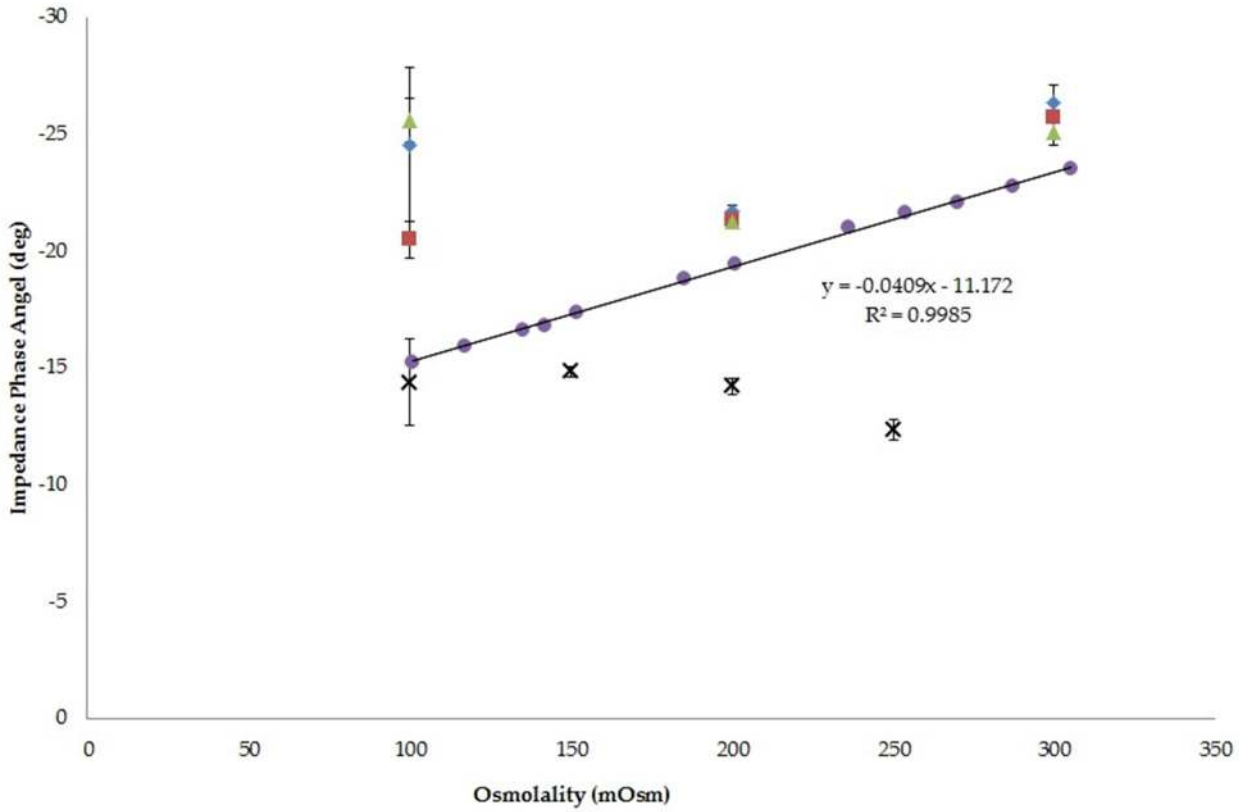

FIGURE 24: The phase angle of the impedance in relation to the osmolality of zebrafish sperm suspended in HBSS at concentrations of $1.4x10^8$ (diamond), $1.05x10^8$ (square), $1.0x10^8$ (X), $7x10^7$ (triangle), and 0 (circle) cells/mL.

Because the phase angle component of the impedance showed sensitivity to the presence of sperm cells, the magnitude component of the impedance recorded during the same studies listed above was compared to the osmolality. The magnitude values behaved in a more stable manner than the phase angle when sperm were present in the sample. The resistance values showed a high variability ($9.6x10^3$ Ω) at 100 mOsm during the experiments with sperm, but this decreased as the experiment progressed (Figure 26). The impedance decreased $1.2x10^4 \pm 1.3x10^3$ Ω to $5.9x10^3 \pm 8$ Ω as the osmolality increased from 100 to 250 mOsm. This is an expected result, as the conductance should increase with the strength of the electrolyte solution, albeit in a non-

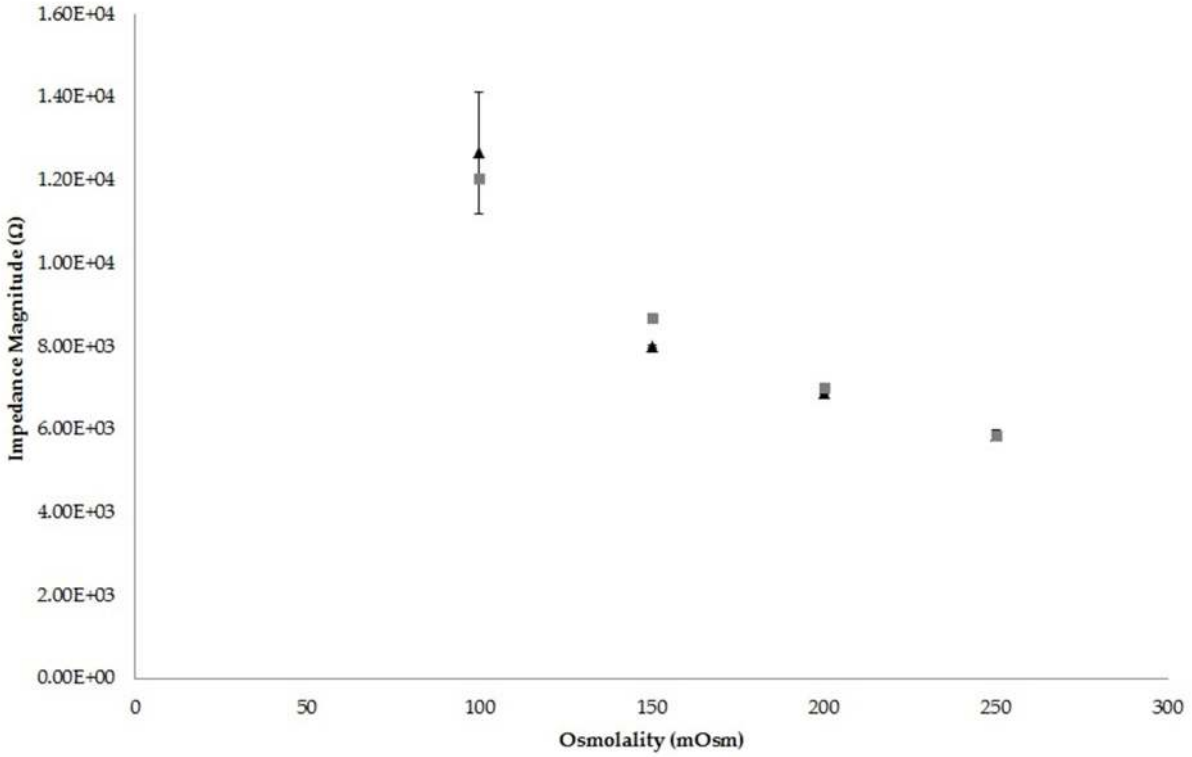

FIGURE 25: A comparison of resistive component of the impedance in relation to the osmolality of a range of HBSS dilutions (grey squares) and zebrafish sperm cells suspended in HBSS (black triangles).

linear fashion. To determine the uncertainty of the sensor response with cells present, the standard curve was fitted with the equation shown in Figure 25, and the impedance variability values were used to determine the resulting variation in osmolality in the range of values tested. Due to the higher variability of impedance at the lower (100 mOsm) range, the osmolality uncertainty was ± 14 mOsm. This uncertainty decreased to ± 7 mOsm at the high (250 mOsm) end of the sensor range. A Student's T-Test ($\alpha = 0.05$) was performed to investigate the statistical significance of the impedance data when cells were present or were absent (Figure 27). The only data pair that showed statistical significance was at 150 mOsm. Considering the magnitude values for each osmolality were similar to each other, the method of using the resistive component of impedance to measure the osmolality of a cell solution on chip was a viable solution.

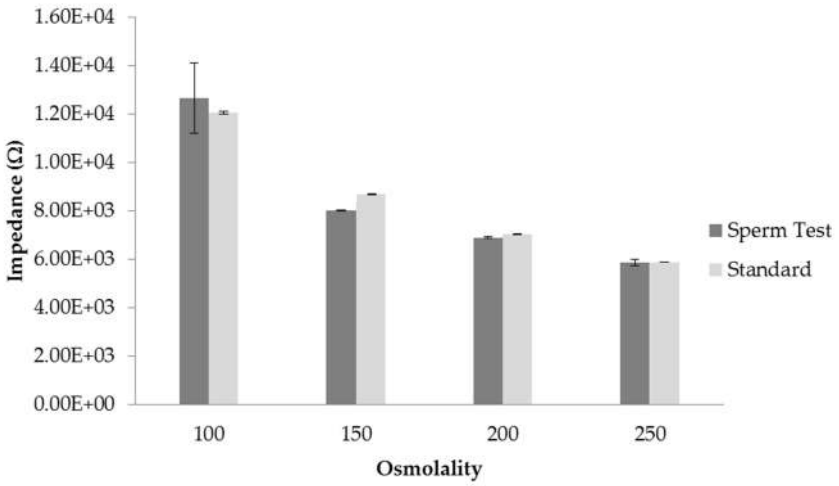

FIGURE 27: Statistical analysis of on-chip osmolality determination between HBSS dilutions and zebrafish sperm suspended in HBSS. * denotes significance (α=0.05, n=3)

The discrepencies in phase angle when comparing the impedance values of HBSS and zebrafish sperm suspended in HBSS can be explained in terms of inductance and capacitance. The phase angle measurements for all tests were negative, indicating that the floor electrode in the device exhibited capacitive behavior. Previous studies have determined that planar electrodes exhibit a double layer capacitance, which influences the impedance signal at frequencies lower than $1x10^5$ Hz (Gawad, Schild et al. 2001, Segerink, Sprenkels et al. 2010). When sperm cells are introduced into the interrogation area of the electrode, the cells interfered with the double layer capacitance of the electrode, thus changing the phase angle. The resistive component of the impedance was likely unaffected due to fact that planar electrodes have been shown to have a small change in resistence (<3%) for particles between 5-8 μm than other electrode configurations (Gawad, Schild et al. 2001). Thus the magnitude of the impedance is affected more by the electrolyte concentration of the solution. All impedance studies done using zebrafish sperm showed the highest standard deviation at 100 mOsm. This was likely due to the lower conductivity of the solution at this concentration, combined with the interference of the sperm cells. However, because studies of the electrical properties of cells in an electrolyte

solution are typically performed in an isotonic environment, further experimentation relating the solution conductivity and the electrical properties of cells is needed. A larger spacing between the electrodes might increase the sensitivity of the real impedance values, as a greater impedance value, and a change in that value, could result from a change in osmolality. However, this larger interrogation volume could also be subject to artifact by the greater likelihood of cells (and/or debris) being present in the interrogation area. Future simulation and experiments exploring optimal electrode and microchannel geometries may prove useful in this regard.

CHAPTER 3: CONCLUSIONS AND FUTURE WORK

3.1 Conclusions

In this study, a microfluidic device with the ability to activate zebrafish sperm for motility analysis and to measure the osmolality of the cell solution in the microchannel was introduced. The on-chip micromixer allowed for reproducible mixing of fluids (57 ± 6 to 94 ± 1% at 3-1 PSI), which resulted in consistent zebrafish sperm cell activation (66 ± 6%). The incorporation of the micromixer removes the possibility of human error associated with hand mixing, lending to the standardization of activation techniques. The incorporation of a simple, pneumatically driven, flow controller in place of a syringe pump facilitated a flow cessation time of ~1 s for all pressures tested. This is 5 fold improvement over previous microfluidic devices used for zebrafish sperm analysis, which had latent periods of 5-10 s after activation before bulk fluid flow subsided (Park, Egnatchik et al. 2012, Scherr, Knapp et al. 2015). More importantly, prompt cessation of flow allowed for motility analysis to be performed during the burst motility phase of activation. This represents an improvement over manual activation methods, which can have a latency period of ~10 s due to procedural requirements and human error. By performing motility analysis on-chip, it was determined that there was a drop in motility from 66 ± 6% to 47 ± 6% during the first 10 s after activation. This equipment free solution to flow control also facilitated the replacement of the syringe pump with PCR microcentrifuge tubes. This design change decreased the volume of the zebrafish sperm sample needed for analysis from ~200 μL to ~60 μL. The on-chip microelectrode allowed for the measurement of the osmolality of a zebrafish sperm sample in the device channel. The capability to measure osmolality on-chip permits the researcher to analyze the osmolality of a sample in real time, which saves time and facilitates the creation of accurate activation curves. Overall, the device described herein has the potential to aid in the standardization of cryopreservation techniques for zebrafish sperm by eliminating the error caused by the human element in experiments involving the investigation sperm motil-

ity and osmolality. Overall, the standardization of motility analysis techniques across research laboratories will offer researchers the capability to reduce the ambiguity in data generated by manual activation methods.

3.2 Future Directions

3.2.1 Device Goals and Proposed Research

Moving forward, it would be useful to further optimize the on-chip electrode for osmolality detection. This would involve investigating new electrode configurations, as well as interrogation techniques. For example, because there was a strong correlation between the resistive component of the impedance values, it may prove beneficial to determine osmolality by measuring the conductivity of the cell solution, as has been reported for on-chip detection of tear osmolality (Jacobi C. 2011). A more thorough design analysis for optimal electrical interrogation of osmolality would be worthwhile, as sensitivity and robustness of the sensing system may be improved with different numbers, geometries and configurations of the electrodes in the microchannel. For instance, the TearLab chip uses a four-electrode configuration (Jacobi C. 2011), and other on-chip electrical sensing studies have shown the difference between floor and side-wall electrode placement (Gawad, Schild et al. 2001). It would also be beneficial to continue the miniaturization of the currently required laboratory equipment into portable apparatuses that can be used with the current chip design, such as the Cheapstat portable potentiostat that could be used for these applications, potentially reducing the overall cost of on-chip osmolality detection. Other off-chip components that should also be considered for further development would be the replacement of the microscope with another optical device such as a cell phone camera and lens system. The iPod 6 used for PTV analysis, could prove to be a viable option. In order to achieve portability, one would have to create a small, but sensitive electrical interrogation apparatus that could connect directly to the on-chip electrode. The end design would be a

true LOC device with the capability to perform sperm analysis in the field or be portable for movement between used aquaculture and research facilities with greater ease.

Beyond on-chip analysis of standard motility as studied in this project, the microfluidic platform may enable new and more powerful studies of aquatic sperm physiology. For instance, because the flow can be directly controlled with greater precision in the microfluidic device than could be accomplished by pipetting onto a microscope slide, more complex studies of sperm swimming behavior, such as rheotactic or chemotactic behavior, could be accomplished, as have been done for other species sperm (El-Sherry, Elsayed et al. 2014, Tung, Ardon et al. 2014). The platform of interrogating sperm visually in the vicinity of electrodes could also be utilized to study sperm swimming behavior in the presence of an electric field, or perhaps sorting sperm using a dielectrophoresis technique as has been done with other cell types in bioMEMS devices (Lee 2016).

3.2.2 Proposed Plan for Large Scale Production

For this device to truly standardize zebrafish sperm activation, it must be made available to the aquaculture research community. Fabrication of the current device design requires specialized equipment and training, and each device can only analyze a limited number of samples (<10) before cell adhesion fouls the device. Using current methods, the time taken to fabricate three devices (assuming the silicon master mold and electrodes are readily available) is approximately 7 hrs. A trained technician can feasibly make 6 chips per day if two wafers are used simultaneously, resulting in approximately 100 devices every 17 days. If the target user group is assumed to be the aquaculture gamete research community (~100 labs), and aquaculture farms specialized in Freshwater Egg Layers (92 farms) (2012 Census of Agriculture, USDA, National Agricultural Statistics Service), and each user were to request 10 chips, it would take approximately 326 days to fabricate enough chips to satisfy this order.

In order to take this device to the manufacturing stage, the design must be re-evaluated and modified to fit the industrial scale. While PDMS on glass devices are useful for research scale prototyping, the current methods for fabricating these devices are not well adapted to the manufacturing scale. Thermoplastics, such as PMMA, polystyrene (PS), and polyethylene terephthalate (PET), are widely used in industry due to their ability to be remolded multiple times after curing by heating the material to its glass transition temperature (Ren, Zhou et al. 2013). These materials are purchased as solids that are then used to fabricate devices using thermomolding. The surface of these materials also retains hydrophilicity after oxygen plasma treatment for up to a few years, possibly eliminating the need for grafting of the hydrophilic PEG-Silane to prevent cell adhesion (Ren, Zhou et al. 2013). There are multiple techniques used in order to seal a thermomolded device to a base, including thermobonding and adhesives (Tsao and DeVoe 2009). The selection of a bonding process would need to be determined experimentally, as all techniques have advantages and disadvantages. Adhesives tend to pose a threat in terms of clogging the channel, and thermobonding has a tendency to deform the channel geometry when the materials are heated to the glass transition temperature. These materials also allow for the easy integration of electrodes (Lin, Jen et al. 2001, Studer, Pépin et al. 2002). Thermomolding is a cheap and rapid manufacturing technique, and requires the use of metal templates, such as brass, that can withstand high temperatures. Because these templates are non-sacrificial and robust, and the device design is likely to remain constant, the most economical option would be to outsource their production.

Large-scale fabrication of devices by thermomolding will require the acquisition of a hot embosser capable of fabricating microfluidic devices. One option is to custom fabricate the equipment to fit the needs of the device. A low-cost template for fabricating a rapid cycle hot embossed has been proposed that uses off-the-shelf parts, has the capability to output one device every two minutes with submicron variatoin, and would cost approximately $10k (Hale

2009). In addition to creating channel geometries, the micro-to-macro interface (inlet/outlet reservoirs and pneumatic bulb) used in the sperm activation device will have to be redesigned to fit the needs of large scale production. These parts will need to be customized so that they do not add considerable time to fabrication. 3-dimensional printing or injection molding are the natural options for fabricating consistent polymer parts. 3-dimensional printing is more cost efficient than injection molding, but can have long fabrication times and poor reproducibility due to environmental conditions. Due to these problems, injection molding would likely be used. There are two options by which this can be implemented: buy an injection molding press, or outsource the production of parts. The decision would require a long-term economic analysis based on the number of chips sold per year and the cost of each method. However, outsourcing may be the best option during the start-up phase of production. Noble Plastics, based out of Grand Coteau, Louisiana, is a product realization company that specializes in injection molding, and may serve as a useful business partner due to the convenience of their location.

Using the methods described above, the production time of sperm activation devices could be reduced considerably. If the total production time for one day is reasonably assumed to be 6 hrs/day, then this fabrication scheme could produce up to 72 devices per day, depending on the methods of bonding and macro-to-micro interface decided upon. This is a 12-fold improvement over the current fabrication method. With the ability to produce a large number of devices in a short period of time, the device could be readily distributed to the aquaculture gamete research community.

REFERENCES

Audiffred, J. (2012). *Label-Free, Single-Cell Viability Detection Using Electrical Impedance and a PMMA Microchip Device*, Louisiana State University.

Beebe, D. J., G. A. Mensing and G. M. Walker (2002). "Physics and applications of microfluidics in biology." *Annu Rev Biomed Eng* **4**: 261-286.

Begolo, S., D. V. Zhukov, D. A. Selck, L. Li and R. F. Ismagilov (2014). "The pumping lid: investigating multi-material 3D printing for equipment-free, programmable generation of positive and negative pressures for microfluidic applications." *Lab Chip*.

Chen, C. Y., L. Y. Cheng, C. C. Hsu and K. Mani (2015). "Microscale flow propulsion through bioinspired and magnetically actuated artificial cilia." *Biomicrofluidics* **9**(3): 11.

Cooper, T. G. and C.-H. Yeung (2006). "Computer-aided evaluation of assessment of "grade a" spermatozoa by experienced technicians." *Fertility and Sterility* **85**(1): 220-224.

Cosson, J. (2004). "The ionic and osmotic factors controlling motility of fish spermatozoa." *Aquaculture International* **12**: 69-85.

Dooley, K. and L. I. Zon (2000). "Zebrafish: a model system for the study of human disease." *Current Opinion in Genetics & Development* **10**(3): 252-256.

Douglas-Hamilton, D. H., K. M. Craig and T. G. Kenny (2011). Computer-aided Semen Analysis. *Cryopreservation in Aquatic Species*. T. R. Tiersch and C. C. Green. Baton Rouge, LA, World Aquaculture Society**:** 6.

Draper, B. W., C. M. McCallum, J. L. Stout, A. J. Slade and C. B. Moens (2004). "A highthroughput method for identifying N-ethyl-N-nitrosourea (ENU)-induced point mutations in zebrafish." *Meth. Cell Biol.* **77**: 440-445.

El-Sherry, T. M., M. Elsayed, H. K. Abdelhafez and M. Abdelgawad (2014). "Characterization of rheotaxis of bull sperm using microfluidics." *Integrative Biology* **6**(12): 1111-1121.

Futai, N., W. Gu and S. Takayama (2004). "Rapid Prototyping of Microstructures with Bell-Shaped Cross-Sections and Its Application to Deformation-Based Microfluidic Valves." *Advanced Materials* **16**(15): 1320-1323.

Gawad, S., L. Schild and P. H. Renaud (2001). "Micromachined impedance spectroscopy flow cytometer for cell analysis and particle sizing." *Lab Chip* **1**(1): 76-82.

Ghosh, S., D. van den Ende, F. Mugele and M. H. G. Duits (2016). "Apparent wall-slip of colloidal hard-sphere suspensions in microchannel flow." *Colloids and Surfaces a-Physicochemical and Engineering Aspects* **491**: 50-56.

Glynn, M. T., D. J. Kinahan and J. Ducree (2014). "Rapid, low-cost and instrument-free CD4+ cell counting for HIV diagnostics in resource-poor settings." *Lab Chip* **14**(15): 2844-2851.

Guerra, S. M., D. G. Valcarce, E. Cabrita and V. Robles (2013). "Analysis of transcripts in gilthead seabream sperm and zebrafish testicular cells: mRNA profile as a predictor of gamete quality." *Aquaculture* **406-407**: 28-33.

Hagedorn, M., J. Ricker, M. McCarthy, S. A. Meyers, T. R. Tiersch, Z. M. Varga and F. W. Kleinhans (2009). "Biophysics of zebrafish (Danio rerio) sperm." *Cryobiology* **58**(1): 12-19.

Hale, M. (2009). *Development of a low-cost, rapid cycle hot embossing system for microscale parts*, Massachusetts Institute of Technology.

Hardt, S., K. S. Drese, V. Hessel and F. Scho¨nfeld (2005). "Passive micromixers for applications in the microreactor and υTAS fields." *Microfluidics and Nanofluidics* **1**(2).

Harvey, B., R. N. Kelley and M. J. Ashwood-Smith (1982). "Cryopreservation of zebrafish spermatozoa using methanol." *Can. J. Zool.* **60**(8): 1867-1870.

Hessel, V., H. Lowe and F. Schonfeld (2005). "Micromixers - a review on passive and active mixing principles." *Chemical Engineering Science* **60**(8-9): 2479-2501.

Hessel, V., H. Löwe and F. Schönfeld (2005). "Micromixers—a review on passive and active mixing principles." *Chemical Engineering Science* **60**(8-9): 2479-2501.

Horsman, K. M., S. L. R. Barker, J. P. Ferrance, K. A. Forrest, K. A. Koen and J. P. Landers (2004). "Separation of Sperm and Epithelial Cells in a Microfabricated Device: Potential Application to Forensic Analysis of Sexual Assault Evidence." *Analytical Chemistry* **77**(3): 742-749.

Irawan, H., V. Vuthiphandchai and S. Nimrat (2010). "The effect of extenders, cryoprotectants and cryopreservation methods on common carp (Cyprinus carpio) sperm." *Anim Reprod Sci* **122**(3-4): 236-243.

Iwai, K., K. C. Shih, X. Lin, T. A. Brubaker, R. D. Sochol and L. Lin (2014). "Finger-powered microfluidic systems using multilayer soft lithography and injection molding processes." *Lab Chip* **14**(19): 3790-3799.

Jacobi C., J. A., Kruse F.E., Cursiefen C. (2011). "Tear film osmolarity measurements in dry eye disease using electrical impedance technology." *Cornia* **30**(12): 1289-1292.

Johnson, T. J., D. Ross and L. E. Locascio (2002). "Rapid Microfluidic Mixing." *Analytical Chemistry* **74**(1): 45-51.

Kime, D. E., K. J. W. Van Look, B. G. McAllister, G. Huyskens, E. Rurangwa and F. Ollevier (2001). "Computer-assisted sperm analysis (CASA) as a tool for monitoring sperm quality in fish." *Comparative Biochemistry and Physiology Part C: Toxicology & Pharmacology* **130**(4): 425-433.

Kovarik, M. L., P. C. Gach, D. M. Ornoff, Y. Wang, J. Balowski, L. Farrag and N. L. Allbritton (2012). "Micro total analysis systems for cell biology and biochemical assays." *Anal Chem* **84**(2): 516-540.

L.I. Segerink, R. J. R., A.J. Sprenkels, I. Vermes, A. van den Berg (2009). "Spermatozoa detection and counting on chip.pdf." *Netherlands Society for Clinical Chemistry and Laboratory Medicine* **34**(4): 254-255.

Lee, D. (2016). "Negative dielectrophoretic force based cell sorter with simplified structure for high reliability." *Int J Precis Eng Manuf* **17**.

Li, W., T. Chen, Z. Chen, P. Fei, Z. Yu, Y. Pang and Y. Huang (2012). "Squeeze-chip: a finger-controlled microfluidic flow network device and its application to biochemical assays." *Lab Chip* **12**(9): 1587-1590.

Lieschke, G. J. and P. D. Currie (2007). "Animal models of human disease: zebrafish swim into view." *Nat Rev Genet* **8**(5): 353-367.

Lin, Y.-C., C.-M. Jen, M.-Y. Huang, C.-Y. Wu and X.-Z. Lin (2001). "Electroporation microchips for continuous gene transfection." *Sensors and Actuators B: Chemical* **79**(2–3): 137-143.

Lopez-Garcia, M. D., R. L. Monson, K. Haubert, M. B. Wheeler and D. J. Beebe (2008). "Sperm motion in a microfluidic fertilization device." *Biomed Microdevices* **10**(5): 709-718.

Macdonald, J. R. (1992). "Impedance Spectroscopy." *Annals of Biomedical Engineering* **20**: 289-305.

MicroChem. "Permanent Epoxy Negative Photoresist Processing Guidelines for SU-2025." from http://www.microchem.com/products/pdf/SU-82000DataSheet2025thru2075Ver4.pdf.

Morris, J. P., S. Berghmans, D. Zahrieh, D. S. Neuberg and J. P. Kanki (2003). "Zebrafish sperm cryopreservation with N,N-dimethylacetimide." *Biotechniques* **35**: 956-958.

Nakagata, N. (2000). "Cryopreservation of mouse spermatozoa." *Mamm Genome* **11**(7): 572-576.

Nguyen, N.-T. and Z. Wu (2005). "Micromixers—a review." *Journal of Micromechanics and Microengineering* **15**(2): R1-R16.

Norris, J. V., M. Evander, K. M. Horsman-Hall, J. Nilsson, T. Laurell and J. P. Landers (2009). "Acoustic differential extraction for forensic analysis of sexual assault evidence." *Anal Chem* **81**(15): 6089-6095.

Park, D. S., R. A. Egnatchik, H. Bordelon, T. R. Tiersch and W. T. Monroe (2012). "Microfluidic mixing for sperm activation and motility analysis of pearl Danio zebrafish." *Theriogenology* **78**(2): 334-344.

Polge, C. and L. E. A. Rowson (1952). "Fertilizing Capacity of Bull Spermatozoa after Freezing at −79° C." *Nature* **169**: 626-627.

Polge, C., A. U. Smith and A. S. Parkes (1949). "Revival of Spermatozoa after Vitrification and Dehydration at Low Temperatures." *Nature* **164**: 666.

Ren, K., J. Zhou and H. Wu (2013). "Materials for Microfluidic Chip Fabrication." *Accounts of Chemical Research* **46**(11): 2396-2406.

Sbalzarini, I. F. and P. Koumoutsakos (2005). "Feature point tracking and trajectory analysis for video imaging in cell biology." *Journal of Structural Biology* **151**(2): 182-195.

Scherr, T., G. L. Knapp, A. Guitreau, D. S. Park, T. Tiersch, K. Nandakumar and W. T. Monroe (2015). "Microfluidics and numerical simulation as methods for standardization of zebrafish sperm cell activation." *Biomed Microdevices* **17**(3): 65.

Scherr, T., C. Quitadamo, P. Tesvich, D. S. Park, T. Tiersch, D. Hayes, J. W. Choi, K. Nandakumar and W. T. Monroe (2012). "A Planar Microfluidic Mixer Based on Logarithmic Spirals." *J Micromech Microeng* **22**(5): 55019.

Scherr, T. F. (2014). *Numerical Modeling of Cryopreserved Zebrafish Sperm Cell Activation In a Microfluidic Device*, Louisiana State University.

Schindelin, J., I. Arganda-Carreras, E. Frise, V. Kaynig, M. Longair, T. Pietzsch, S. Preibisch, C. Rueden, S. Saalfeld, B. Schmid, J.-Y. Tinevez, D. J. White, V. Hartenstein, K. Eliceiri, P. Tomancak and A. Cardona (2012). "Fiji: an open-source platform for biological-image analysis." *Nat Meth* **9**(7): 676-682.

Segerink, L. I., A. J. Sprenkels, P. M. ter Braak, I. Vermes and A. van den Berg (2010). "On-chip determination of spermatozoa concentration using electrical impedance measurements." *Lab Chip* **10**(8): 1018-1024.

Seguin, C., J. M. McLachlan, P. R. Norton and F. Lagugne-Labarthet (2010). "Surface modification of poly(dimethylsiloxane) for microfluidic assay applications." *Applied Surface Science* **256**(8): 2524-2531.

Seo, D. B., Y. Agca, Z. C. Feng and J. K. Critser (2007). "Development of sorting, aligning, and orienting motile sperm using microfluidic device operated by hydrostatic pressure." *Microfluidics and Nanofluidics* **3**(5): 561-570.

Sood, R., M. A. English, M. Jones, J. Mullikin, D. M. Wang, M. Anderson, D. Wu, S. C. Chandrasekharappa, J. Yu, J. Zhang and P. Paul Liu (2006). "Methods for reverse genetic screening in zebrafish by resequencing and TILLING." *Methods* **39**(3): 220-227.

Stroock, A. D., S. K. Dertinger, A. Ajdari, I. Mezic, H. A. Stone and G. M. Whitesides (2002). "Chaotic mixer for microchannels." *Science* **295**(5555): 647-651.

Studer, V., A. Pépin, Y. Chen and A. Ajdari (2002). "Fabrication of microfluidic devices for AC electrokinetic fluid pumping." *Microelectronic Engineering* **61–62**: 915-920.

Suh, R. S., X. Y. Zhu, N. Phadke, D. A. Ohl, S. Takayama and G. D. Smith (2006). "IVF within microfluidic channels requires lower total numbers and lower concentrations of sperm." *Human Reproduction* **21**(2): 477-483.

Sui, G., J. Wang, C.-C. Lee, W. Lu, S. P. Lee, J. V. Leyton, A. M. Wu and H.-R. Tseng (2006). "Solution-Phase Surface Modification in Intact Poly(dimethylsiloxane) Microfluidic Channels." *Analytical Chemistry* **78**(15): 5543-5551.

Tabeling, P. (2005). *Introduction To Microfluidics*. United States, Oxford University Press Inc.

Tiersch, T. R., H. Yang, J. A. Jenkins and Q. Dong (2007). "Sperm cryopreservation in fish and shellfish." *Soc Reprod Fertil Suppl* **65**: 493-508.

Tsao, C.-W. and D. L. DeVoe (2009). "Bonding of thermoplastic polymer microfluidics." *Microfluidics and Nanofluidics* **6**(1): 1-16.

Tung, C. K., F. Ardon, A. G. Fiore, S. S. Suarez and M. Wu (2014). "Cooperative roles of biological flow and surface topography in guiding sperm migration revealed by a microfluidic model." *Lab Chip* **14**(7): 1348-1356.

Whitesides, G. M. (2006). "The origins and the future of microfluidics." *Nature* **442**(7101): 368-373.

Wilson-Leedy, J. G. and R. L. Ingermann (2007). "Development of a novel CASA system based on open source software for characterization of zebrafish sperm motility parameters." *Theriogenology* **67**(3): 661-672.

Wilson-Leedy, J. G., M. K. Kanuga and R. L. Ingermann (2009). "Influence of osmolality and ions on the activation and characeteristics of zebrafish sperm motility." *Theriogenology* **71**: 1054-1062.

Wolenski, J. S. and N. H. Hart (1987). "Scanning electron microscope studies of sperm incorporation into the zebrafish (Brachydanio) egg." *Journal of Experimental Zoology* **243**(2): 259-273.

Yang, H., C. Carmichael, Z. M. Varga and T. R. Tiersch (2007). "Development of a simplified and standardized protocol with potential for high-throughput for sperm cryopreservation in zebrafish Danio rerio." *Theriogenology* **68**(2): 128-136.

Yang, H. and T. R. Tiersch (2009). "Current status of sperm cryopreservation in biomedical research fish models: zebrafish, medaka, and Xiphophorus." *Comp Biochem Physiol C Toxicol Pharmacol* **149**(2): 224-232.

Yang, H. and T. R. Tiersch (2011). Sperm Cryopreservation in Biomedical Reserach Fish Models. *Cryopreservation in Aquatic Species, 2nd Edition*. T. R. a. C. C. G. Tiersch. Baton Rouge, Louisiana, World Aquaculture Society**:** 439-454.

Zhou, J., A. V. Ellis and N. H. Voelcker (2010). "Recent developments in PDMS surface modification for microfluidic devices." *Electrophoresis* **31**(1): 2-16.

Zhou, J., D. A. Khodakov, A. V. Ellis and N. H. Voelcker (2012). "Surface modification for PDMS-based microfluidic devices." *Electrophoresis* **33**(1): 89-104.

APPENDIX

APPENDIX A: CRYOPRESERVATION OF ZEBRAFISH SPERM

Cryopreservation is the act of freezing germplasm of a desired species to a state of suspended animation for storage, with the intent of thawing and reanimating the resources for later use. This is accomplished through a series of steps including: sample collection, sperm diluting (extension), the selection and addition of cryoprotectants, cooling, storage, thawing, and viability detection. Each of these steps must be carefully developed, optimized, and investigated to prevent accumulation of even small losses at each step (Yang, Carmichael et al. 2007).

Cryopreservation has been applied to the conservation of genetic resources in numerous species such as cattle *(Bos Taurus)* (Polge and Rowson 1952) laboratory mice *(Mus musculus)* (Polge, Smith et al. 1949), and most notably in humans *(Homo sapians)* (Nakagata 2000). While these studies serve as examples for the utility of cryopreservation, a lack of standardized protocols for zebrafish sperm preservation has resulted in a multitude of complications. One difficulty that occurs during cryopreservation is the generation of ice crystals caused by freezing water. When these crystals form within the cells, the membrane integrity of the cell can be compromised. In order to reduce the creation of ice crystals, cryoprotectants are added to reduce the intracellular freezing point (Yang and Tiersch 2011). Common cryoprotectants include methanol, glycerol, N,N-dimethyl acetamide (DMA) and dimethyl sulfoxide (DMSO) among others (Irawan, Vuthiphandchai et al. 2010). The use of cryoprotectants has been shown to be effective; however, chemical ratios and concentrations vary between species due to varying sperm size, concentration, and physiology. Because of this variation, optimal cryoprotectant techniques must be established experimentally (Yang and Tiersch 2009). Although cryopreservation protocols for zebrafish sperm exist (Morris, Berghmans et al. 2003, Draper, McCallum et al. 2004, Sood, English et al. 2006) most are based on a single protocol from over 30 years ago (Harvey, Kelley et al. 1982) and yield inconsistent results (Hagedorn, Ricker et al. 2009). These

ambiguities have resulted in a lack of cohesive knowledge on the true effects of a multitude of cryopreservation variables on the quality of post-thaw zebrafish sperm. For example, there was an observed variation in post-thaw fertility (33 ± 20% with a range of 5-81%) in zebrafish sperm samples with the same initial percent motility that were frozen using the same cryopreservation protocol (Yang, Carmichael et al. 2007). To reduce the variability in these results, protocols for cryopreservation need refinement and evaluation using pre-freeze and post-thaw motility studies. One necessary step in creating a standardized cryopreservation protocol for zebrafish is to develop a simple and reproducible means to evaluating sperm quality before and after freezing (Yang and Tiersch 2009).

APPENDIX B: STANDARD OPERATING PROCEDURES

SOP-1:Hanks' balanced salt solution (HBSS)

Hanks' balanced salt solution is used as a collection medium for sperm. The HBSS should be prepared with an osmolality of 290 to 300 mOsmol/Kg to prevent activation of the sperm.

Procedure:

1. Combine the ingredients (Table A-1) with distilled water; bring the total volume to ~ 3.9 L.

2. Stir until all solutes are dissolved.

3. Verify the osmolality of mixture using osmometer; adjust to 300 mOsmol/kg by adding water.

4. Distribute the solution into 1 -L bottles, and label with the date and name of person preparing the solution.

5. Store bottles in refrigerator.

TABLE A.1 Ingredients for Hanks' balanced salt solution.

Ingredient	grams/Liter	Molarity
NaCl	8.00	0.1400
KCl	0.40	0.0050
CaCl2•2H2O	0.16	0.0010
MgSO4•7H2O	0.20	0.0010
Na2HPO4	0.06	0.0004
KH2PO4	0.06	0.0004
NaHCO3	0.35	0.0040
C6H12O6(glucose)	1.00	0.0060

Tiersch, T. R., Goudie, C. A. & Carmichael, G. J. 1994. Cryopreservation of channel catfish sperm: storage in cryoprotectants, fertilization trials, and growth of channel catfish produced with cryopreserved sperm. *Transactions of the American Fisheries Society*, 123: 580-586.

SOP-2: Use of the osmometer Osmette III™

1. OBJECTIVE

To reliably measure the osmotic strength of a solution, colloid or compound using the osmometer Osmette III™.

2. HEALTH AND SAFETY

Closed-toed shoes, laboratory coat, and eye protection must be worn in the laboratory.

3. PERSONNEL/TRAINING RESPONSIBILITIES

After reading these procedures, have assisted-training from experienced staff.

4. REQUIRED AND RECOMMENDED MATERIALS

All materials are located in room 121C:

- Osmette III pipette (silver) - top drawer on the left plastic organizer
- Pipette tips – top cabinet
- Cleanette absorbent cleaning rod
- Standard solutions – top cabinet
- Osmometry standard bottles labeled with different osmolarities – top cabinet
- Kimwipes®

5. TO MAINTAIN THE ACCURACY OF THE STANDARDS

5.1 Standards should be stored at room temperature with the caps or pour spouts tightly closed.

5.2 Pour, do NOT pipette, from the bottle into a clean, dry microcentrifuge tube. Pipette from this tube.

5.3 Replace cap immediately. Standards and samples will change their values fairly quickly if left uncovered.

5.4 Do NOT dilute contents.

5.5 Discard solution after use; NEVER return it to the bottle.

5.6 Discard the bottle when only 20% of the contents remain.

5.7 Use care in opening ampoules to avoid sharp edges.

5.8 When pipetting the sample, there should be an air separation between the sample and the Teflon piston tip. Careless pipetting will result in erroneous readings.

6. TURNING ON AND CALIBRATION

6.1 Switch ON/OFF switch to ON, and allow the cooler to cool down.

6.2 Push a cleanette all the way to the bottom of the *cooler well*. Rotate it to remove any moisture. Remove and dispose it. Repeat this procedure after every run.

6.3 Every time the osmometer is turned ON, calibration needs to be checked. If drifting, recalibrate.

6.4 After the display has cycled, using the pipette with a clean, dry pipette tip, pick up 10 µl of a 100 mOsm sample and place the pipette tip into the *cooler well*.

6.5 DO NOT PIPPETE THE SAMPLE INTO THE WELL!! The sample remains in the pipette tip with handle attached during the measurement cycle. Do NOT press the

plunger of the pipette handle while the pipette tip is in the *well*, or probe damage may result.

6.6 Always wipe the outside of the pipette tip dry with a Kimwipe® before inserting the tip into the *well*.

6.7 Press RUN. The osmometer will countdown to zero to freeze, and then will give an osmolarity measurement. Running this sample will clean the *well* and ensure the electronics and cooler are cycling correctly.

6.8 Press the CAL button (Fig. 1) to start a new calibration.

Fig. 1. Pressure sensitive key pad.

6.9 The message on the screen will change from *Wipe before sample* to *Wipe before STD*.

6.10 Wipe the well with a *cleanette* before each standard is run.

- Run three replicates of deionized water samples (0 mOsm)
- Run three replicates of 100 mOsm standards
- Run three replicates of 500 mOsm standards
- Run three replicates of 1500 mOsm standards
- Run three replicates of 2000 mOsm standards

6.11 Place a fresh pipette tip containing each standard into the *cooler well* and press RUN.

6.12 Observe the Display. Seeding (vibration) will occur when Display reads 0. After READ is displayed, the reading for that Standard is automatically added to the calibration.

6.13 Press CAL to end and save the new calibration.

6.14 If the following error message occurs: OUTSIDE CALIBRATION, possible fixes are:

- Recalibrate using previous standards and one higher if the reading was above the maximum previous standard.
- Recalibrate using previous standards and one lower if the reading was be-

low the minimum previous standard.

6.15 In addition to the 125-ml bottles of standards, CON-TROL™ Reference Standards are available in 5-ml glass ampoules for 100, 290 and 500 mOsm/kg. Check the standards against the CON-TROL™ Reference Standards every week or two, depending on the load of samples tested each week.

7. RUNNING OF SAMPLES

7.1 Once the osmometer is calibrated, pipette the solution to be tested, wipe the tip and place the pipette tip with handle attached in the *cooler well*.

7.2 Always wipe the outside of the pipette tip dry with a Kimwipe® before inserting the tip into the *well*.

7.3 Press RUN. The osmometer will countdown to zero to freeze, and then will give an osmolarity measurement.

7.4 Make sure that the *cooler well* is cleaned with a cleanette AFTER EACH RUN.

7.5 Once all the samples are analyzed, switch ON/OFF switch to OFF. The *cooler well* will close automatically.

8. FACTORS AFFECTING REPRODUCIBILITY

8.1 Always use the pipette tips and cleanettes provided by the vendor.

8.2 Carefully pipette samples to avoid capturing air in the bottom of the pipette tip. NOTE: There SHOULD be air between the sample and the Teflon plunger.

8.3 Make sure pipette tips fit snug on the Teflon plunger. If they do not fit, it may be that the Teflon tip is worn out and needs replacement.

8.4 Storing pipette with the tip cover will help increase the lifespan of the Teflon tip.

8.5 When Teflon tip is worn out, sample may leak into the well, giving inconsistent readings

8.6 Run a series of samples or standards in quick succession, discarding the first reading, as it thermally conditions the *well*.

8.7 Avoid re-running the sample with the same pipette tip.

9. LITERATURE

Osmette III™, Model 5010 Automatic Osmometer, Operating Manual. 2008. Precision Systems Inc. Natick, MA.

APPENDIX C: BODE PLOT

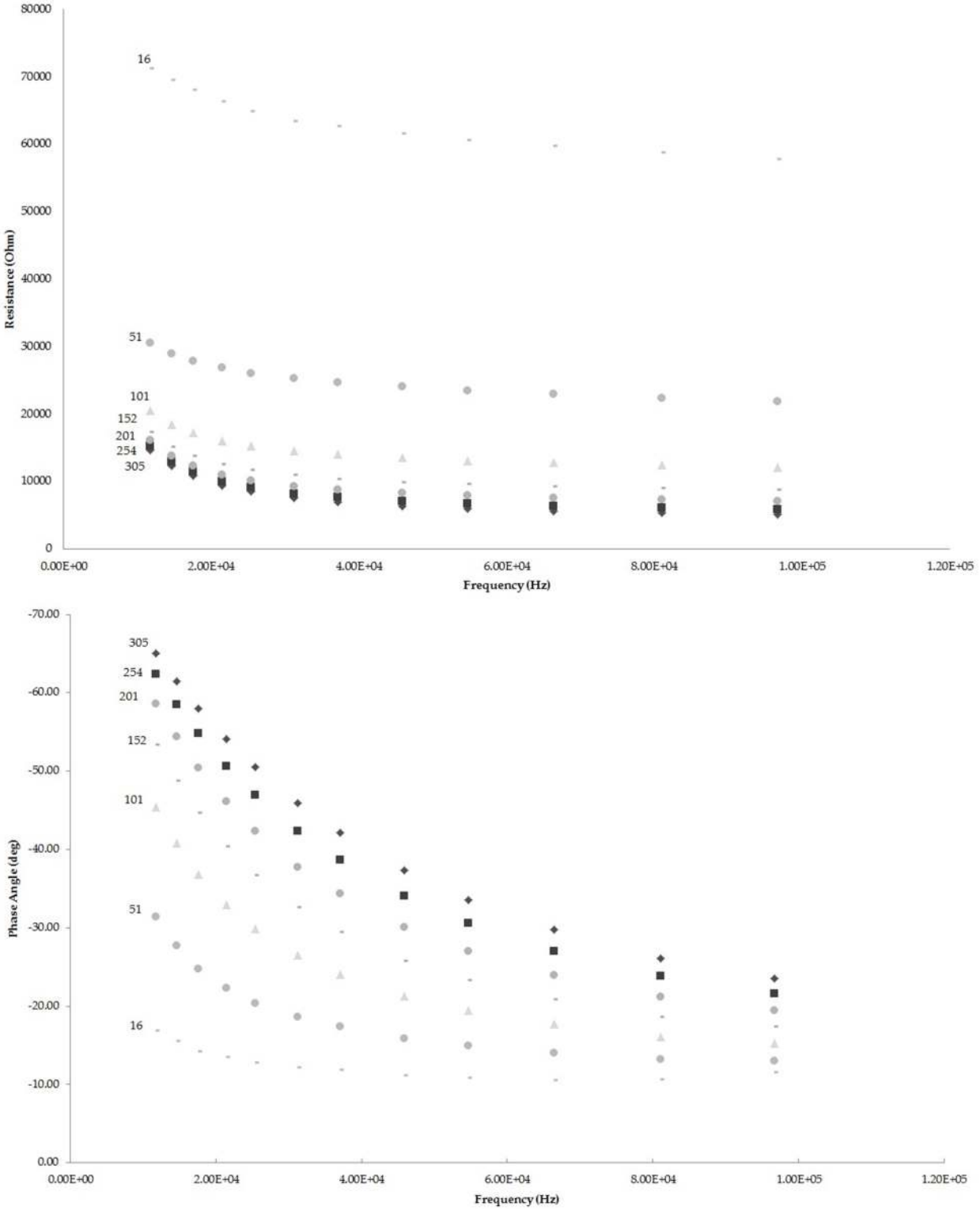

Figure A1: The frequency response for (Top) the magnitude and (Bottom) the phase angle of the impedance as osmolality is increased from 16-305 mOsm. Each point represent the mean ± S.D. of three aliquots from each dilution of HBSS.

VITA

Jacob Beckham is a native of Baytown, Texas. He received his B.S. in Biological and Agricultural Engineering from Louisiana State University in 2013. In June 2013, he enrolled in the graduate program in the Department of Biological Engineering at Louisiana State University to pursue a Master's degree in Biological Engineering, which is anticipated to be awarded in August 2016.